SIXTH EUROPEAN ROTORCRAFT AND POWERED LIFT AIRCRAFT FORUM

Paper N° 46

EXPERIMENTAL AND THEORETICAL STUDIES ON HELICOPTER BLADE TIPS AT ONERA

Jean-Jacques Philippe and Jean-Jacques Chattot

Office National d'Etudes et de Recherches Aérospatiales (ONERA)
92320 Châtillon (FRANCE)

September 16-19, 1980

Bristol, England

THE UNIVERSITY, BRISTOL, BS8 1HR, ENGLAND

EXPERIMENTAL AND THEORETICAL STUDIES ON HELICOPTER BLADE TIPS AT ONERA*

by Jean-Jacques Philippe and Jean-Jacques Chattot

Office National d'Etudes et de Recherches Aérospatiales
(ONERA)
92320 Châtillon (FRANCE)

SUMMARY

In a first part, the working conditions of helicopter rotor blade tips are briefly recalled. In the second part, the simplified case is studied of a non-lifting rotor, for which ONERA possesses a large number of test results and a first computing programme adapted to almost arbitrary blade shapes. This programme is described in detail and the first results are presented. The last part presents some experimental results of absolute pressure distributions on the straight tips of a twisted rotor, and brings to light the influence of the wind tunnel velocity, of the lift and propulsive forces generated by the rotor on the local forces applied on the blade tips. A sweptback parabolic tip has been defined with a view to reduce the effects of the transonic flow on the advancing blade; wind tunnel tests show that it improves the total performance of the rotor relative to a reference one equipped with conventional straight tips.

I - INTRODUCTION

For many years ONERA is active in the field of helicopter rotor aerodynamics, on both experimental and theoretical viewpoints [1]. The present paper concerns studies on blade tips, except as regards the aspects related to studies of new profiles specific to helicopter blades, which are the subject of another paper [2] . The research effort for improving the knowledge and prediction of the flow over blade tips has been carried out in close connexion with the Aérospatiale Company, but also within the framework of cooperative agreements with the U.S. Army (USARTL).

In the first part, we briefly recall the working conditions of the blade tips of a helicopter rotor. In the second part, we study the simplified case of a non-lifting rotor, for which we have now available a large number of test results and a first computer programme adapted to an almost arbitrary shape of blade;

* Studied carried out with the financial support of the Technical Service of Aeronautical Programmes, French Ministry of Defence.

this programme will be described in detail. The unsteady solutions obtained to date will be compared with available experimental results, but also commented in relation with quasi-steady results obtained by RAE and NASA.

In the last part, we approach the study of blade tips in the real case with lift; to this end, we present experimental results on pressure distributions obtained on a wind tunnel model. A sweptback parabolic tip has been defined with a view to reduce the effects of transonic flows on the advancing blade; the results on the total performance of a rotor equipped with these tips are finally compared with those of a reference rotor equipped with conventional straight tips.

2 - RECALL OF AERODYNAMIC WORKING CONDITIONS OF BLADE TIPS

The combination of the helicopter forward speed and the uniform rotation of the rotor entails that each blade section is attacked at a velocity whose normal component to the blade span varies as a sine function of time $(\omega r + V_0 \sin \psi)$. There also appears a radial velocity $V_0 \cos \psi$ (parallel to the blade span), directed towards the outside of the rotor disc for the rear part of the disc (ψ varying from 270° to 90°, passing through zero), and towards the inside of the rotor disc for the front part of the disc (ψ varying between 90° and 270°, passing through 180°). To compensate the asymmetry of the attack velocities between the sector of advancing blade, where the forward velocity and the rotor rotating velocity are added, and the sector of retreating blade where these velocities are subtracted, and to ensure the balance in roll of the rotor, the angles of attack must be small on the advancing blade and large on the retreating blade.

Figures 1 and 2 show the lines of iso-Mach, iso-sweep angle and iso-incidence, obtained by a calculation performed by the method of acceleration potential developed at ONERA [3] . In this calculation it has been taken into account, to find the local incidence, the non-linearities experimentally observed during tests on the profiles used for the rotor. It is a flight configuration of Dauphin SA 365 at 265 km/h and 2000 m altitude, for a mass of 3000 kg (the tip speed of the rotor has been taken at 220 m/sec, which corresponds to an advance ratio (μ equal to 0.335).

We shall remark that, even at this moderate velocity of 265 km/h, the incoming Mach number on the advancing blade exceeds 0.8 at the tip, and is associated with slightly positive incidences. If we tried to increase the helicopter speed, the tip of the advancing blade would be in severe transonic flow conditions, at zero or slightly negative incidence. In this sector of advancing blade, the tips would have a large drag, and the power necessary for driving the rotor would increase very much for a slight increase of forward speed.

$\mu = 0.335$ $V_0 = 73.7$ m/sec $\omega R = 220$ m/ sec Flight altitude $\approx$ 2000 m

Iso- mach lines | Iso-sweep (φ) angle lines

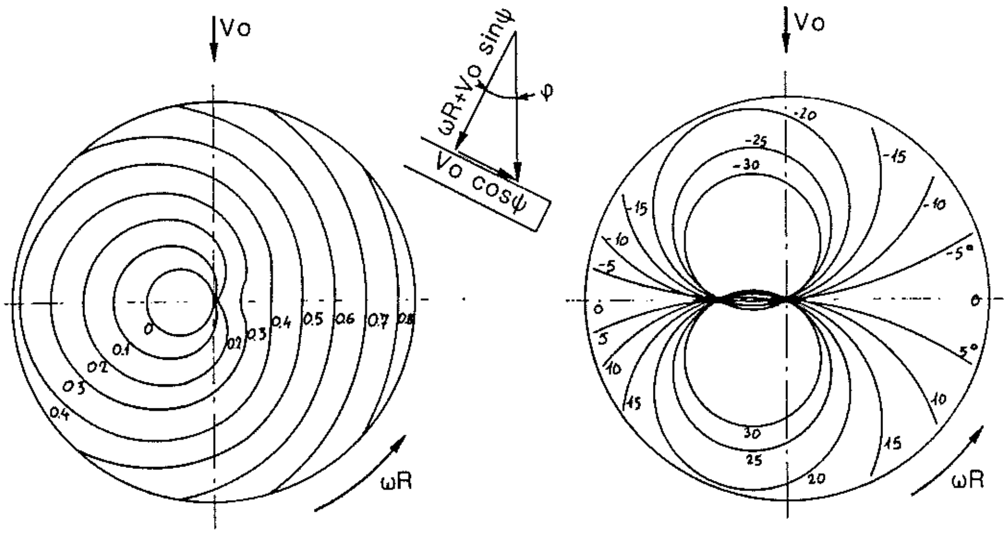

Figure 1 - Iso-Mach lines and Iso-sweep-angle lines

$V_0 = 73.7$ m/sec $\omega R = 220$ m/sec $\mu = 0.335$

Mass = 3000 kg Flight altitude $\approx$ 2000 m

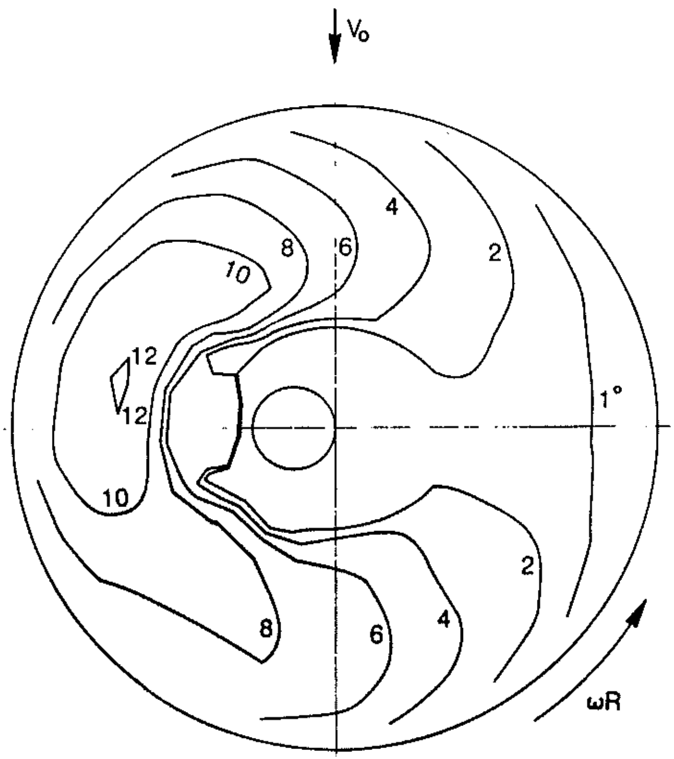

Figure 2 - Iso-incidence lines.

That is why the studies conducted up to now concerned mainly the unsteady transonic flows occurring on the advancing blade, and more particularly in the case of a non lifting rotor as, within a broad azimuthal sector of advancing blade, the blade tips have an incidence close to zero.

3 - IDEAL CASE OF A NON LIFTING ROTOR

With a view to better understand the effects of unsteady three-dimensional flows on the pressure distributions over helicopter rotor blades, tests and calculations have been performed for the "simplified" case of a non lifting rotor (symmetric, non-twisted blade at zero angle of attack).

3.1 - Brief recall of experimental results acquired at ONERA

From 1975 onwards, tests have been carried out at the S2 Chalais-Meudon wind tunnel on a two-bladed, non-twisted rotor with symmetric profiles of the NACA 00XX family. The removable blade tips, starting at 0.8 R, were equipped with absolute pressure transducers. The reference straight tip has a 0.75 m radius and is trapezoidal (c = 0.166 m at 0.37 R and 0.115 m at R). The profile relative thickness decreases linearly from 17% at 0.37 R to 14.5% at 0.8 R, then down to 9% at the tip. The results obtained on this straight blade have been described in detail in Ref. [4] , and figure 3 recalls one of the main conclusions of this study. There is a marked asymmetry between the pressure distributions measured at 0.9 R for two azimuths symmetric about 90° as soon as transonic flows are present on the blade, and this asymmetry is all the more marked as the advance ratio μ is larger. An increasing incident Mach number (before azimuth 90°) is favourable for delaying the onset of shocks; inversely a decreasing Mach number (after ψ = 90°) is unfavourable, generating very severe shock waves. Around the blade tip there is also a marked influence of radial flow, on which we shall come back later.

Many other results have also been acquired on this same rotor, equipped, this time, with a 30°-sweep tip. During these tests, the rotor radius has been increased to 0.835 m by addition of an 85 mm part, with NACA 0014.5 profile, between 0.719 and 0.820 R. The comparative study of the straight and swept tips has been presented in Ref. [5], and figure 4 recalls its main conclusions : the swept tip is better over a broad sector of advancing blade (up to about 120° for the 0.9 R section), but we should note that it is not always beneficial in the external region of the tip, where strong reaccelerations of the flow appear, as found also in the following calculations.

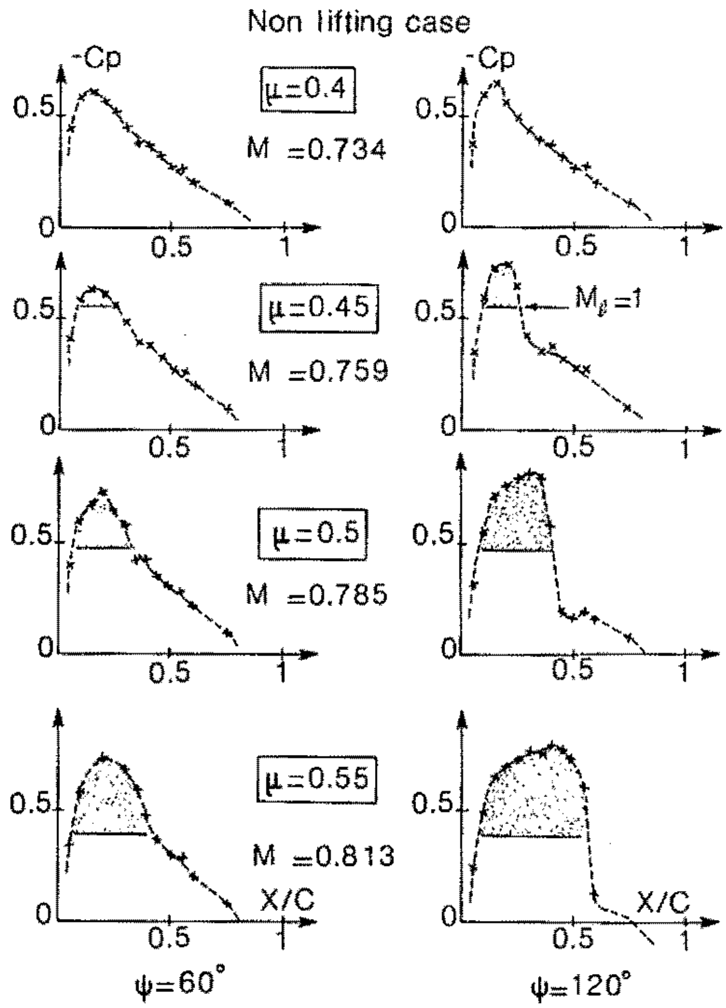

Figure 3 - Experimental evolution of pressure distributions with the advance ratio. ($\omega R = 200 m/sec$)

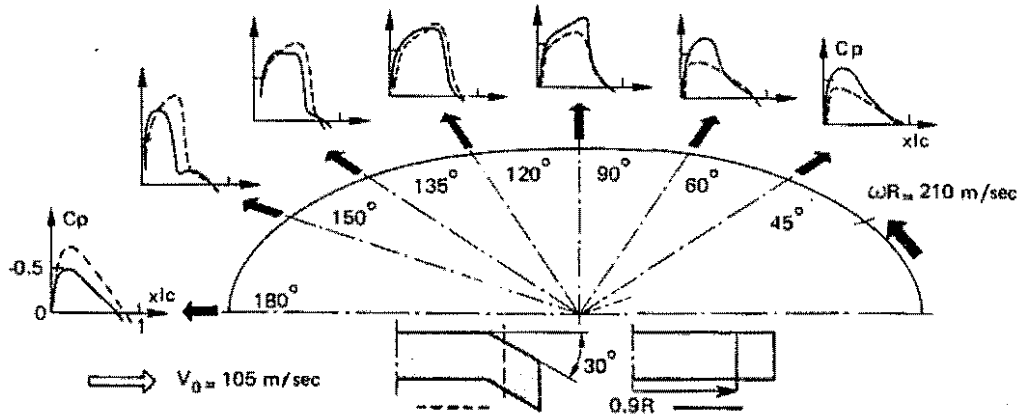

Figure 4 - Evolution of pressure distributions on rotor blade tips, non lifting case. NACA 0012 section at 0.9R.

3.2 - Method used for three-dimensional, transonic, unsteady flow calculations.

3.2.1 - Equation of unsteady transonic small perturbations

Considering the existing computing means and the performance of the resolution methods, the modeling of the physical phenomena taking place on a helicopter blade tip is realized within the simplified scheme of an ideal fluid theory taking account of shock waves when these are weak enough for the entropy variations to be neglected. The transonic flows having a more marked unsteady character than purely subsonic or supersonic ones (the propagation speed of wave fronts $|u-a|$ being small relative to $|U|$), this aspect had to be properly treated, which is only possible in the case of a conservative equation ensuring the correct propagation speed of the shock waves. That is why the equation of unsteady, transonic, small perturbations, written for low frequencies (a hypothesis justified for helicopters by Isom [6]), has been chosen as mathematical model.

In a blade attached Cartesian coordinate system, this equation writes :

$$(1)\qquad A\frac{\partial^2\phi}{\partial t\partial x}=\frac{\partial}{\partial x}\left[B\frac{\partial\phi}{\partial x}+B'\left(\frac{\partial\phi}{\partial x}\right)^2\right]+C\frac{\partial^2\phi}{\partial x\partial y}+D\frac{\partial^2\phi}{\partial y^2}+E\frac{\partial^2\phi}{\partial z^2}$$

The hypothesis leading to its derivation are :

$$1-M'^2\ (1+\mu)^2=O(\delta^{2/3})$$
$$\varepsilon=O(\delta)$$

where : $M'=\omega R/a_\infty$ is the rotational Mach number at the blade tip,

δ the relative thickness of the blade reference profile,

$\varepsilon=c/R=1/\lambda$ the inverse of the blade aspect ratio.

The coefficients of the equation depend on y and on the azimuthal position ψ or, which is equivalent, on a dimensionless time t , but not on the velocity :

$$A=2M'^2\frac{\varepsilon}{\delta^{2/3}}\,(y+\mu\cos t)$$

$$B=\frac{1-M'^2\,(y+\mu\cos t)^2}{\delta^{2/3}}$$

$$C=2M'^2\frac{\varepsilon}{\delta^{2/3}}\ \mu\sin t\ (y+\mu\cos t)$$

$$D=\frac{\varepsilon^2}{\delta^{2/3}}$$

$$E=1$$

The passage from physical variables (overlined) to dimensionless variables is made by means of the following relations (x chordwise, y spanwise) :

$t = \psi^\circ - 90^\circ = \omega \bar{t}$

$x = \dfrac{\bar{x}}{c}$

$y = \dfrac{\bar{y}}{R}$

$z = \delta^{1/3} \dfrac{\bar{z}}{c}$

$\phi = \delta^{-2/3} \left\{ \dfrac{\bar{\phi}}{\bar{u}_\infty c} - \dfrac{\bar{x}}{c} \right\}$ $\qquad \bar{u}_\infty = \omega r + V_o \sin\psi$

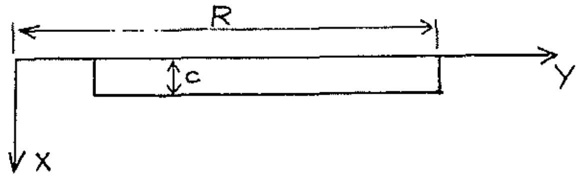

Equation (1) is hyperbolic in time. The steady part is non-linear and of mixed type. Let $\beta = B + 2B' \partial\phi/\partial X$ be the coefficient of $\partial^2\phi/\partial X^2$ of the equation in developed form. The three possible situations are the following :

- $\beta > 0$; the steady equation is of elliptic type, corresponding to a subsonic flow,
- $\beta < 0$; the equation is hyperbolic, corresponding to a locally supersonic flow,
- $\beta = 0$; the equation is parabolic, and the corresponding surface is the sonic surface.

To this equation must be added initial and boundary conditions.

3.2.2 - Initial and boundary conditions

The calculation of the flow past the advancing blade is performed between azimuths ψ = 0 and 180° (t = -90° to +90°). We usually obtain an initial condition at ψ = 0 (t = -90°) by calculating the quasi steady solution corresponding to $\partial^2\phi/\partial t\,\partial X = 0$. In this zone of the rotor disc, the flow is entirely subsonic and the quasi steady and unsteady solutions are very close. The quasi steady solution is obtained by time integration of Eq.(1), but while maintaining the coefficients of the equation fixed at their values corresponding to azimuth ψ = 0. To accelerate convergence, a sequence of time step Δt in geometric progression, constructed on the values Δt_{min} and Δt_{max} of this parameter, is used. The large values of Δt favour the convergence of the modes of large wavelength, and the small values those of the modes of short wavelength [7] .

On the blade or, which is equivalent in the small perturbation theory, on the median surface of the blade in the plane z = 0, we write a tangency condition :

$$\left.\frac{\partial\phi}{\partial z}\right|_{z=0} = (y + \mu \cos t)\, F'_X(x,y)$$

where $\bar{z} = c\delta F(x,y)$ represents the equation of the upper, or lower, surface of the blade.

The first surface of calculation on the blade is located at $y_n = 0.5$. It is classical to write a condition expressing the independence of the solution with respect to y in the form $\left.\partial^2\phi/\partial y^2\right|_{y_n} = 0$.

At a large distance, on the boundaries of the numerical domain, one should apply non-reflexion conditions which would allow the perturbation fronts to come out of the domain. Such conditions however are difficult to write, except at the downstream boundary where they take the simple form $\partial\phi/\partial n = 0$; so we used Dirichlet conditions on those boundaries, compatible with the steady far field solution $\phi = 0$.

Downstream, on the boundary $X = X_X$, we write $\left.\frac{\partial\phi}{\partial X}\right|_{X_X} = 0$.

The effect of the position of the boundaries on the unsteady solution still remains to be ascertained. For the given number of coordinated surfaces in each direction and due to their concentration close to the blade, the external boundaries have been positioned respectively at :

$$x_n = -8 \qquad x_X = 6$$
$$y_n = 0{,}5 \qquad y_X = 1{,}5$$
$$z_n = -3 \qquad z_X = 3$$

3.2.3 - Transformation of coordinates

In order to take into account a blade tip of arbitrary shape, use is made of a transformation of coordinates aligning the prolonged blade leading and trailing edges with coordinated surfaces. It is then possible to treat the boundary conditions as simply as for a rectangular blade. Moreover, the transformation makes it possible to introduce clustering of the mesh in regions where the solution presents strong gradients (leading edge, blade tip, etc.). Figure 5 shows a detail of the mesh system for a blade with sweptback parabolic tip, for which calculation results will be presented in section 4.2.

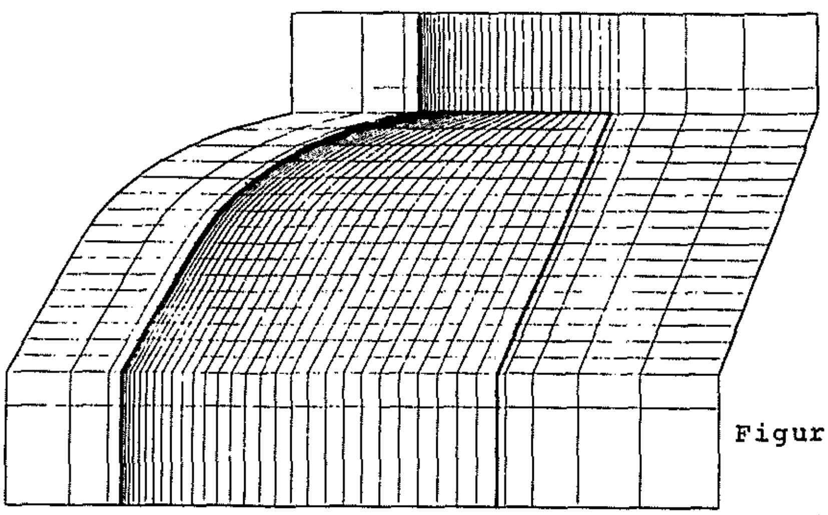

Figure 5 - Detail of the mesh system for the sweptback parabolic tip

The transformation used has the general form :

$$\xi = \xi(x,y)$$
$$\eta = \eta(y)$$
$$\zeta = \zeta(z)$$

Equation (1) writes, in the new coordinates :

$$
\begin{aligned}
A \frac{\partial \xi}{\partial x} \frac{\partial^2 \phi}{\partial t \partial \xi} = {} & B\left(\frac{\partial \xi}{\partial x}\right)^2 \frac{\partial^2 \phi}{\partial \xi^2} + B'\left(\frac{\partial \xi}{\partial x}\right)^3 \frac{\partial}{\partial \xi}\left(\frac{\partial \phi}{\partial \xi}\right)^2 + \left[C \frac{\partial \xi}{\partial x}\frac{\partial \xi}{\partial y} + D\left(\frac{\partial \xi}{\partial y}\right)^2\right]\frac{\partial^2 \phi}{\partial \xi^2} \\
& + \left[C \frac{\partial \xi}{\partial x}\frac{\partial \eta}{\partial y} + 2D \frac{\partial \xi}{\partial y}\frac{\partial \eta}{\partial y}\right]\frac{\partial^2 \phi}{\partial \xi \partial \eta} + D\left(\frac{\partial \eta}{\partial y}\right)^2 \frac{\partial^2 \phi}{\partial \eta^2} + E\left(\frac{\partial \zeta}{\partial z}\right)^2 \frac{\partial^2 \phi}{\partial \zeta^2} \qquad (2) \\
& + B \frac{\partial^2 \xi}{\partial x^2}\frac{\partial \phi}{\partial \xi} + 2B' \frac{\partial \xi}{\partial x}\frac{\partial^2 \xi}{\partial x^2}\left(\frac{\partial \phi}{\partial \xi}\right)^2 + \left[C \frac{\partial^2 \xi}{\partial x \partial y} + D \frac{\partial^2 \xi}{\partial y^2}\right]\frac{\partial \phi}{\partial \xi} + D \frac{\partial^2 \eta}{\partial y^2}\frac{\partial \phi}{\partial \eta} + E \frac{\partial^2 \zeta}{\partial z^2}\frac{\partial \phi}{\partial \zeta}
\end{aligned}
$$

The partial derivatives of the transformation appear in the coefficients of Eq.(2). This semi-conservative form, in which the metric coefficients are written in front of the derivation symbols $\partial/\partial\xi$, $\partial/\partial\eta$, $\partial/\partial\zeta$, makes it possible to preserve, when the transformation is regular enough, the jump conditions associated with the conservative form.

There remains to specify how we can calculate the four first partial derivatives and the five second partial derivatives.

The identities :

$$
\begin{aligned}
x &= x\left[\xi(x,y),\ \eta(y)\right] \\
y &= y\left[\eta(y)\right] \\
z &= z\left[\zeta(z)\right]
\end{aligned}
$$

provide the four following relations :

$$
\begin{aligned}
1 &= \frac{\partial x}{\partial \xi}\frac{\partial \xi}{\partial x} \\
0 &= \frac{\partial x}{\partial \xi}\frac{\partial \xi}{\partial y} + \frac{\partial x}{\partial \eta}\frac{\partial \eta}{\partial y} \\
1 &= \frac{\partial y}{\partial \eta}\frac{\partial \eta}{\partial y} \\
1 &= \frac{\partial z}{\partial \zeta}\frac{\partial \zeta}{\partial z}
\end{aligned}
$$

in which the coefficients $\partial x/\partial\xi$, $\partial x/\partial\eta$, $\partial y/\partial\eta$, $\partial z/\partial\zeta$, can be calculated by the usual centred finite difference second order accurate scheme, e.g. :

$$\left(\frac{\partial x}{\partial \xi}\right)_{i,j} = \frac{X_{i+1,j} - X_{i-1,j}}{2\Delta\xi} + O(\Delta\xi^2)$$

The same above identities allow writing five relations for the second partial derivatives :

$$
\begin{aligned}
0 &= \frac{\partial x}{\partial \xi}\frac{\partial^2 \xi}{\partial x^2} + \frac{\partial^2 x}{\partial \xi^2}\left(\frac{\partial \xi}{\partial x}\right)^2 \\
0 &= \frac{\partial x}{\partial \xi}\frac{\partial^2 \xi}{\partial x \partial y} + \frac{\partial^2 x}{\partial \xi^2}\frac{\partial \xi}{\partial x}\frac{\partial \xi}{\partial y} + \frac{\partial^2 x}{\partial \xi \partial \eta}\frac{\partial \xi}{\partial x}\frac{\partial \eta}{\partial y}
\end{aligned}
$$

$$0 = \frac{\partial x}{\partial \xi}\frac{\partial^2 \xi}{\partial y^2} + \frac{\partial x}{\partial \eta}\frac{\partial^2 \eta}{\partial y^2} + \frac{\partial^2 x}{\partial \xi^2}\left(\frac{\partial \xi}{\partial y}\right)^2 + 2\,\frac{\partial^2 x}{\partial \xi \partial \eta}\frac{\partial \xi}{\partial y}\frac{\partial \eta}{\partial y} + \frac{\partial^2 x}{\partial \eta^2}\left(\frac{\partial \eta}{\partial y}\right)^2$$

$$0 = \frac{\partial y}{\partial \eta}\frac{\partial^2 \eta}{\partial y^2} + \frac{\partial^2 y}{\partial \eta^2}\left(\frac{\partial \eta}{\partial y}\right)^2$$

$$0 = \frac{\partial z}{\partial \zeta}\frac{\partial^2 \zeta}{\partial z^2} + \frac{\partial^2 z}{\partial \zeta^2}\left(\frac{\partial \zeta}{\partial z}\right)^2$$

The coefficients $\partial^2 x/\partial\xi^2, \partial^2 x/\partial\xi\partial\eta, \partial^2 x/\partial\eta^2, \partial^2 y/\partial\eta^2, \partial^2 z/\partial\zeta^2$ are also calculated by finite differences, e.g. :

$$\left(\frac{\partial^2 x}{\partial \xi^2}\right)_{i,j} = \frac{x_{i+1,j} - 2x_{i,j} + x_{i-1,j}}{\Delta\xi^2} + O(\Delta\xi^2)$$

With this mode of calculation of partial derivatives it is easy to verify that any function $\phi = ax + by + cz$ where a, b, c are constants, satisfies identically the equation as well as its discretized form, which we shall now describe.

3.2.4 - Discretization scheme

The discretization of the non-linear term of Eq.(1) is now classical, with the mixed conservative scheme of Murman [8]. We used in the same manner a four-operator scheme, but with a slightly different discretization for the sonic point. According to the sign of β_i and β_{i-1} we may distinguish, for the discretization of $\partial/\partial x\left[B\,\partial\phi/\partial x + B'(\partial\phi/\partial x)^2\right]$ in Cartesian coordinates (the extension to curvilinear coordinates is straight forward) :

- i - $\beta_i \geqslant 0 \quad \beta_{i-1} \geqslant 0$ (subsonic point)

  discretization : $\beta_i \dfrac{\phi_{i+1} - 2\phi_i + \phi_{i-1}}{\Delta x^2}$

(subscripts j and k, which are invariant, are not written)

- ii - $\beta_i < 0 \quad \beta_{i-1} < 0$ (supersonic point)

  discretization : $\beta_{i-1} \dfrac{\phi_i - 2\phi_{i-1} + \phi_{i-2}}{\Delta x^2}$

- iii - $\beta_i < 0 \quad \beta_{i-1} \geqslant 0$ (sonic point)

  discretization : $\beta_i \dfrac{\phi_i - 2\phi_{i-1} + \phi_{i-2}}{\Delta x^2}$

- vi - $\beta_i \geqslant 0 \quad \beta_{i-1} < 0$ (shock point)

  discretization : $\beta_i \dfrac{\phi_{i+1} - 2\phi_i + \phi_{i-1}}{\Delta x^2} + \beta_{i-1}\dfrac{\phi_i - 2\phi_{i-1} + \phi_{i-2}}{\Delta x^2}$

The Murman discretization at the sonic point consists in writing $\beta_i = 0$. Scheme (iii) eliminates spurious oscillations appearing in the viscinity of the sonic line when it lies in a region of strong gradient, which is the case, in particular, at the leading edge of a blunt-nosed profile. The above scheme is not strictly conservative, but the conservation error is small $O(\Delta x)$ and, moreover, the solution is very regular.

The cross derivative term, negligible near the rotor axis, has an important influence towards the blade tip, where radial flows are responsible for a large part of three-dimensional effects. Also, this term is augmented by a contribution $2D\,\partial\xi/\partial y\,\partial\eta/\partial y$ from the second derivatives term, $\partial^2/\partial y^2$, when the blade tip has sweep (Eq.2). With a view to improve the stability of the scheme for a given time step, or to increase the time step while maintaining the stability, we use an upwind scheme according to the sign of the cross derivative coefficient. For the Cartesian form of the equation, the discretization of $C\,\partial^2\phi/\partial x\partial y$ writes :

i - if $C_j \geqslant 0$ (negative sweep relative to mesh system)

discretization : $C_j \dfrac{\phi_{i,j+1} - \phi_{i,j} - \phi_{i-1,j+1} + \phi_{i-1,j}}{\Delta x \Delta y}$

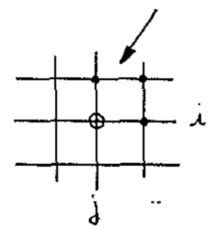

ii - if $C_j < 0$ (positive sweep relative to mesh system)

discretization : $C_j \dfrac{\phi_{i,j} - \phi_{i,j-1} - \phi_{i-1,j} + \phi_{i-1,j-1}}{\Delta x \Delta y}$

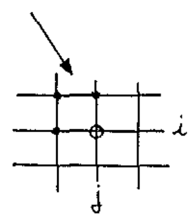

These schemes are easily extended to the case of curvilinear coordinates.

Lastly, the terms $D\,\partial^2\phi/\partial y^2 + E\,\partial^2\phi/\partial z^2$ are discretized by means of centred schemes at every point.

3.2.5 - Resolution algorithm

The time integration of the equation is achieved by means of an Alternating Direction Implicit (ADI) method, which splits the three-dimensional problem into three one-dimensional problems in each coordinate direction. The advantage of such a method is its stability, which can be proved in the case of a linear equation regardless of the Courant number (CFL). Indeed, when solving a complicated problem, with a mesh system where cell sizes may vary by one or more orders of magnitude, it would be very penalizing to limit the time step as a function of a stability criterion associated with the smallest cell.

On the other hand, as Eq.(1) is non-linear, there exists a practical limitation which may be associated with the shedding of vortices at the trailing edge of a lifting profile or the motion of the shock waves.

The three steps of the ADI method using the Crank-Nickolson scheme centred at level n + 1/2 are as follows :

1st step :

$$A \frac{\partial \xi}{\partial x} \frac{\partial}{\partial \xi}\left(\frac{\tilde{\phi}-\phi^n}{\Delta t}\right) = \frac{B}{2}\left(\frac{\partial \xi}{\partial x}\right)^2\left(\frac{\partial^2 \phi^n}{\partial \xi^2}+\frac{\partial^2 \tilde{\phi}}{\partial \xi^2}\right) + B'\left(\frac{\partial \xi}{\partial x}\right)^3 \frac{\partial}{\partial \xi}\left(\frac{\partial \phi^n}{\partial \xi}\frac{\partial \tilde{\phi}}{\partial \xi}\right) + \frac{D}{2}\left(\frac{\partial \xi}{\partial y}\right)^2\left(\frac{\partial^2 \phi^n}{\partial \xi^2}+\frac{\partial^2 \tilde{\phi}}{\partial \xi^2}\right)$$

$$+ \underline{C \frac{\partial \xi}{\partial x}\frac{\partial \xi}{\partial y}\frac{\partial^2 \phi^n}{\partial \xi^2}} + \left(C \frac{\partial \xi}{\partial x}\frac{\partial \eta}{\partial y} + 2D \frac{\partial \xi}{\partial y}\frac{\partial \eta}{\partial y}\right)\frac{\partial^2 \phi^n}{\partial \xi \partial \eta} + D\left(\frac{\partial \eta}{\partial y}\right)^2 \frac{\partial^2 \phi^n}{\partial \eta^2} + E\left(\frac{\partial \zeta}{\partial z}\right)^2 \frac{\partial^2 \phi^n}{\partial \zeta^2}$$

$$+ \frac{B}{2}\frac{\partial^2 \xi}{\partial x^2}\left(\frac{\partial \phi^n}{\partial \xi}+\frac{\partial \tilde{\phi}}{\partial \xi}\right) + 2B'\frac{\partial \xi}{\partial x}\frac{\partial^2 \xi}{\partial x^2}\frac{\partial \phi^n}{\partial \xi}\frac{\partial \tilde{\phi}}{\partial \xi} + \frac{D}{2}\frac{\partial^2 \xi}{\partial y^2}\left(\frac{\partial \phi^n}{\partial \xi}+\frac{\partial \tilde{\phi}}{\partial \xi}\right)$$

$$+ \underline{C \frac{\partial^2 \xi}{\partial x \partial y}\frac{\partial \phi^n}{\partial \xi}} + D\frac{\partial^2 \eta}{\partial y^2}\frac{\partial \phi^n}{\partial \eta} + E\frac{\partial^2 \zeta}{\partial z^2}\frac{\partial \phi^n}{\partial \zeta}$$

It should be noted that the underlined terms are the only ones whose treatment is explicit. It would be possible to use a mixed implicit scheme according to the sign of $C \frac{\partial \xi}{\partial x}\frac{\partial \eta}{\partial y}$. Tests on a swept blade showed that this term has a small influence on stability.

2nd step :

$$A \frac{\partial \xi}{\partial x}\frac{\partial}{\partial \xi}\left(\frac{\tilde{\tilde{\phi}}-\tilde{\phi}}{\Delta t}\right) = \frac{1}{2}\left(C\frac{\partial \xi}{\partial x}\frac{\partial \eta}{\partial y} + 2D\frac{\partial \xi}{\partial y}\frac{\partial \eta}{\partial y}\right)\left(\frac{\partial^2 \tilde{\tilde{\phi}}}{\partial \xi \partial \eta} - \frac{\partial^2 \phi^n}{\partial \xi \partial \eta}\right)$$

$$+ \frac{D}{2}\left(\frac{\partial \eta}{\partial y}\right)^2\left(\frac{\partial^2 \tilde{\tilde{\phi}}}{\partial \eta^2} - \frac{\partial^2 \phi^n}{\partial \eta^2}\right) + \frac{D}{2}\frac{\partial^2 \eta}{\partial y^2}\left(\frac{\partial \tilde{\tilde{\phi}}}{\partial \eta} - \frac{\partial \phi^n}{\partial \eta}\right)$$

3rd step :

$$A \frac{\partial \xi}{\partial x}\frac{\partial}{\partial \xi}\left(\frac{\phi^{n+1}-\tilde{\tilde{\phi}}}{\Delta t}\right) = \frac{E}{2}\left(\frac{\partial \zeta}{\partial z}\right)^2\left(\frac{\partial^2 \phi^{n+1}}{\partial \zeta^2} - \frac{\partial^2 \phi^n}{\partial \zeta^2}\right) + \frac{E}{2}\frac{\partial^2 \zeta}{\partial z^2}\left(\frac{\partial \phi^{n+1}}{\partial \zeta} - \frac{\partial \phi^n}{\partial \zeta}\right)$$

Considering the above schemes, the algebraic systems to be solved for each step have matrices with three or four diagonals, the main diagonal being, by construction of the schemes, usable as a pivot for the Gauss method of elimination.

Each complete solution corresponding to a time step requires 2.5 seconds CPU of CDC 7600 computer for a mesh system of $64 \times 32 \times 16 \simeq 35\ 000$ points.

3.3 - Application of the method to a straight blade

The above numerical method has been applied to a straight blade such as that described in section 3.1. Various calculations have been performed, which emphasize the same phenomena :

- influence of the unsteady term, which delays the appearance of shocks,

- favourable influence of the negative aerodynamic sweep angle, which reduces the pressure peaks at the leading edge.

To illustrate this first point, let us consider (fig. 6) the distribution of Mach number (i.e. of pressure) on the straight blade at azimuths 60° and 120°. The blade is attacked by flows having the same normal Mach number. However, at ψ = 60° the supersonic zone is developing and the shock wave has not yet formed.

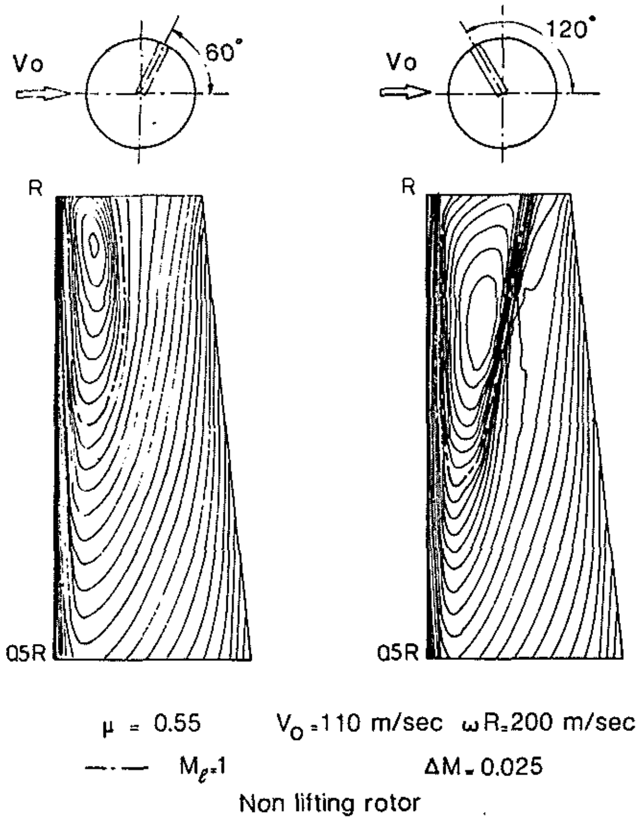

Figure 6 - Straight tip. Iso-Mach lines.

On the other hand, at 120° the supersonic zone and the shock are established. Again we find this asymmetry between the results at azimuths ψ and 180° - ψ on figure 7, where the maximum Mach number is represented as a function of span.

These theoretical results are compared on figure 8 with experimental results obtained at the ONERA S2Ch wind tunnel, for azimuths 60, 90 and 120°. We shall note the excellent agreement between these results.

In order to evaluate the influence of the unsteady term and of the cross derivative term (modeling the radial flows), quasi steady calculations $\partial^2\phi/\partial t\partial x = 0$, have been performed at ψ = 60° and 120°. We shall note (fig.9) the importance of the unsteady term by comparing the unsteady and quasi steady results for the same azimuths on the one hand, and on the other hand the influence of radial flow by comparing the two quasi steady results at 60° and 120° for which the boundary conditions and the equation coefficients are the same, except the cross derivative coefficients which are opposite : C (120°) = -C (60°).

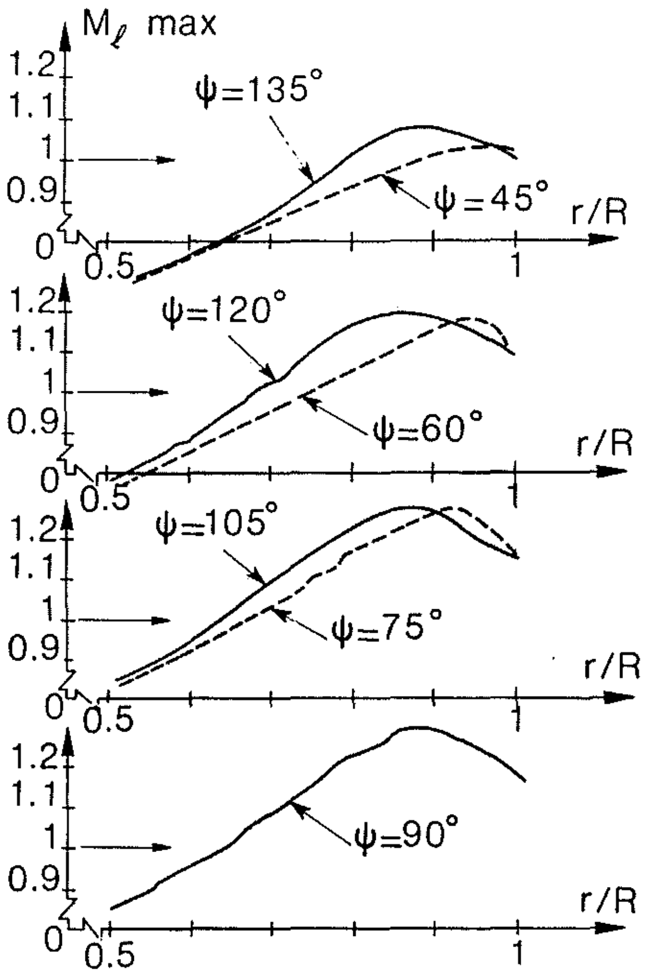

Figure 7 - Spanwise variation of maximum Mach number. Straight tip.

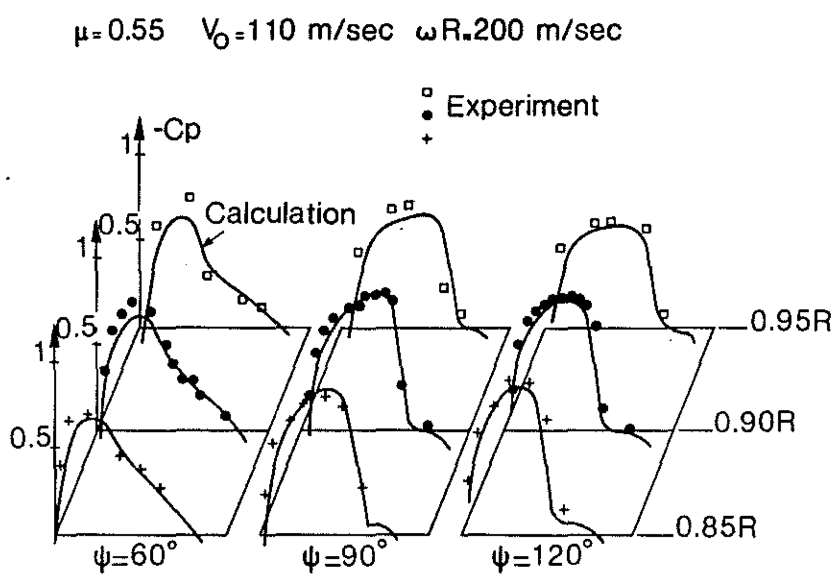

Figure 8 - Comparison between calculation and experiment. Straight tip. Non lifting rotor.

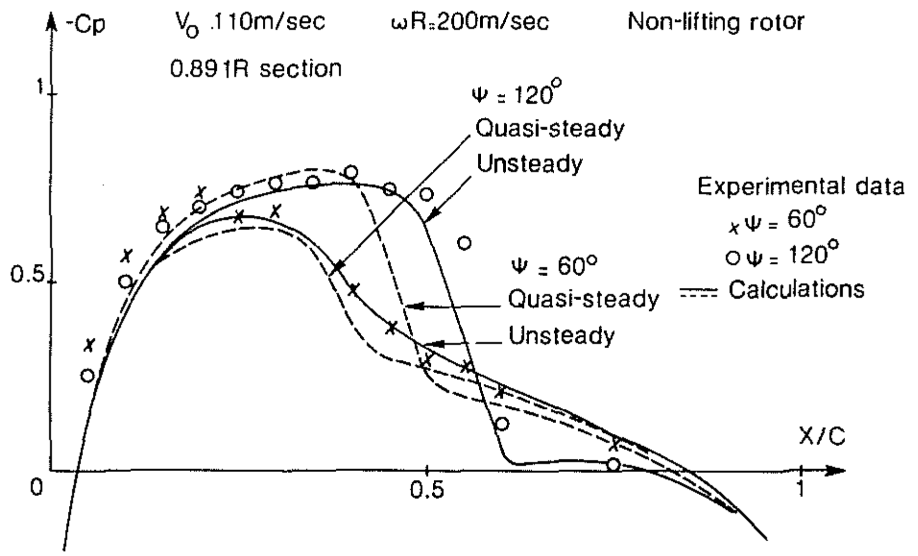

Figure 9 - Influence of the unsteady term and radial term in the model equation near the tip.

The aerodynamic attack with negative sweep tends to attenuate the expansion at the leading edge, and hence to reduce the supersonic zones and the intensity of the recompression shocks.

These two conclusions, drawn from the analysis of results in the spanwise section y = 0.891 R, are found even more clearly in the 0.946 R section, where the more important supersonic zones amplify the phenomena previously described (fig. 10).

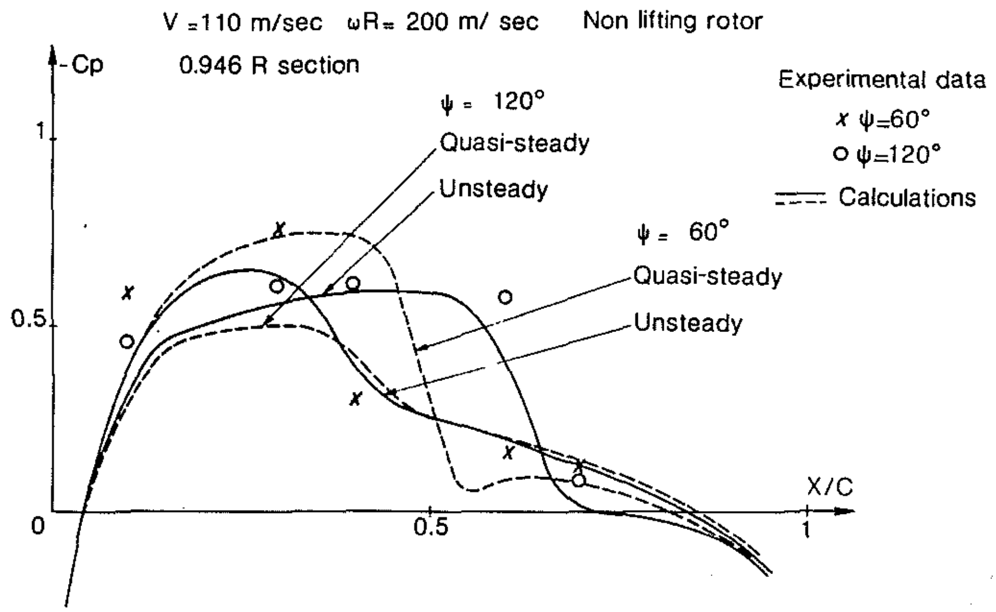

Figure 10 - Influence of the unsteady term and radial term in the model equation very close to the tip.

The sweep angle effect has been confirmed during the calculation of a half wing of aspect ratio $\lambda = 6$, with a NACA 0012 profile and set in yaw in a flow at a Mach number of 0.85 (fig.11). Each calculation required 400 quasi steady iterations, followed by 180 unsteady steps ($\Delta\Psi = 1°$), i.e. a total computing time of 25 mn CPU on CDC 7600.

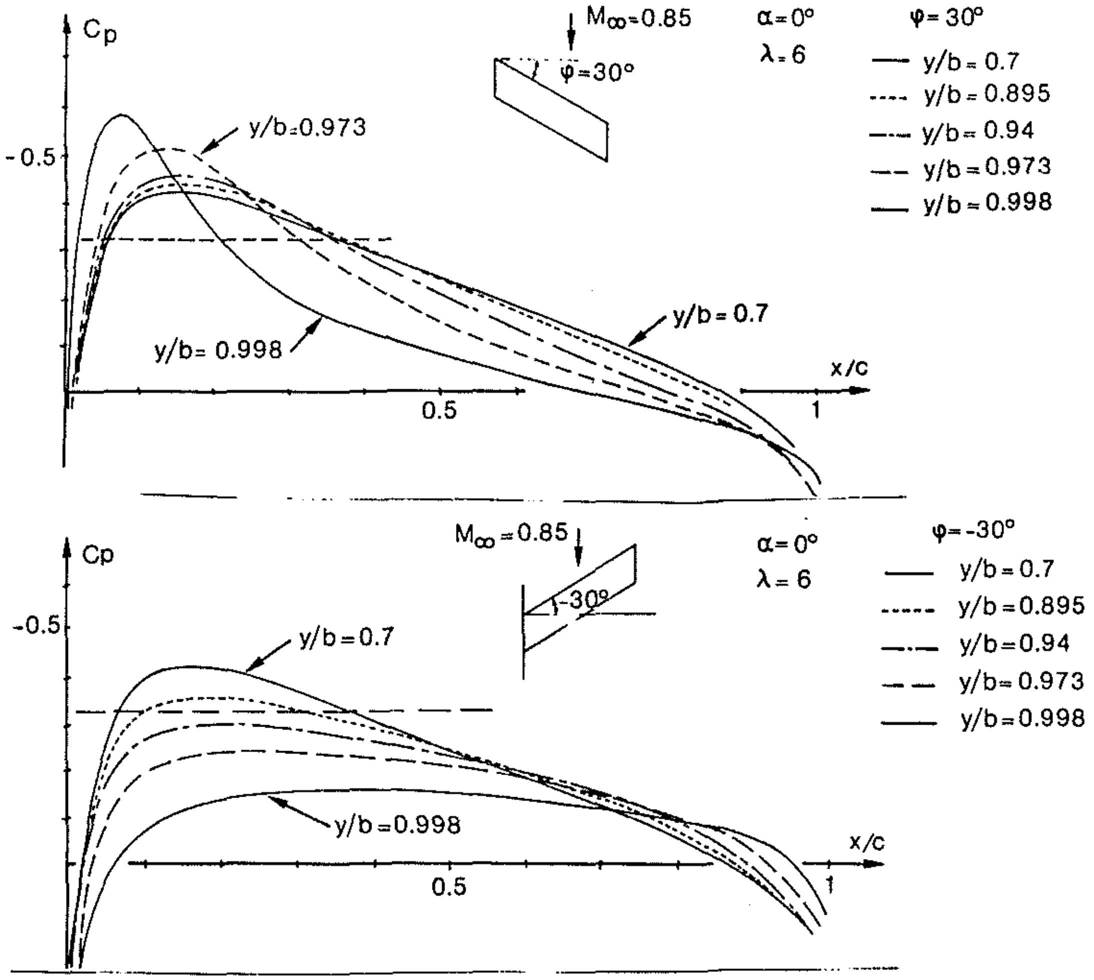

Figure 11 - Effect of positive or negative sweep on half-wing.

3.4 - Application of the method to a blade with 30° swept tip

The study of a swept tip aimed at bringing to light the favourable influence, for the helicopter blade as for the aircraft wing of a diminution of Mach number normal to the leading edge. However, contrary to the aircraft in cruise flight, the blade meets during a cycle an incident flow whose aerodynamic sweep angle varies (see fig.1).

As with the straight tip, the results at azimuths 60° and 120° (fig.12) reveal an asymmetry corresponding to the delay in the shock wave onset. But the detailed analysis of the very complex flow on this blade shows that the tip is subject to a strong expansion, visible on the plotting of maximum spanwise Mach number (fig. 13). The comparison, on this plotting, of the straight and swept tips shows a considerable gain, starting around 0.75 R and especially important towards 0.9 - 0.95 R.

Over the last 5 to 10% of the blade there is an inversion of the effect. To eliminate these overexpansions at the blade tip, a parabolic shape will be defined in section 4.2.

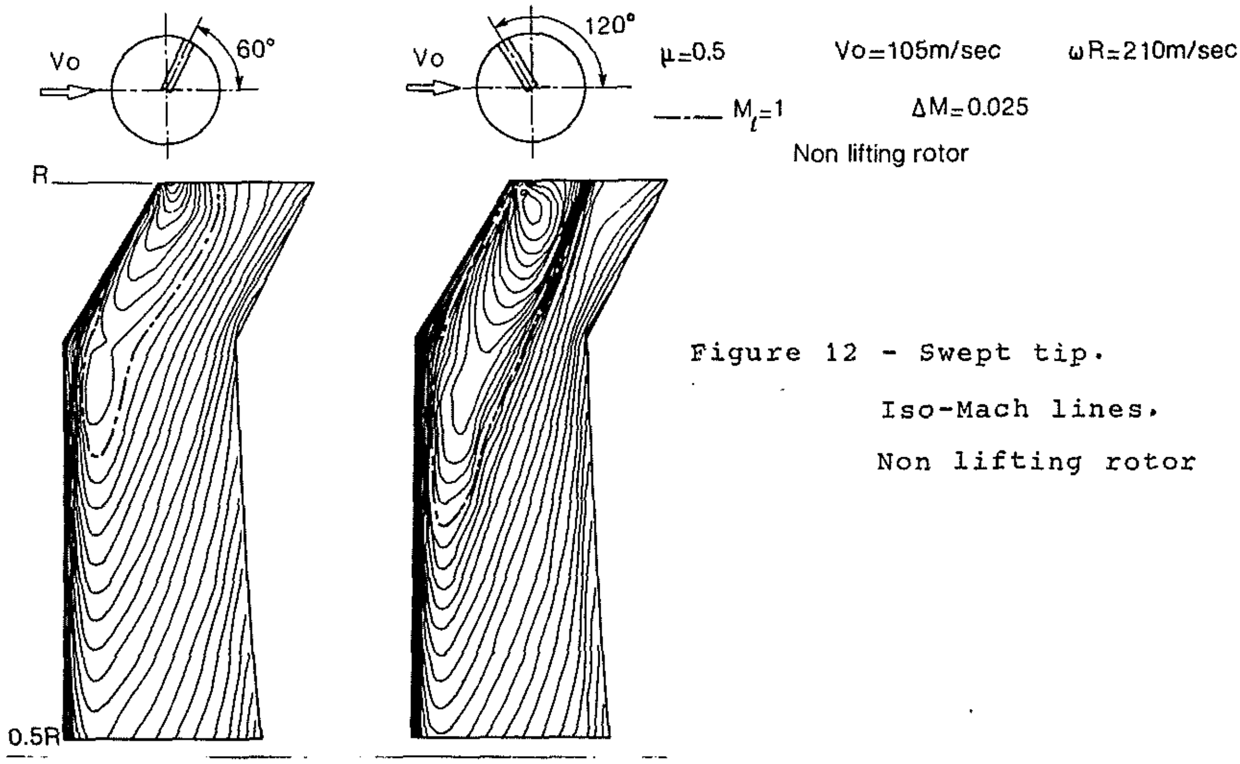

Figure 12 - Swept tip.

Iso-Mach lines.

Non lifting rotor

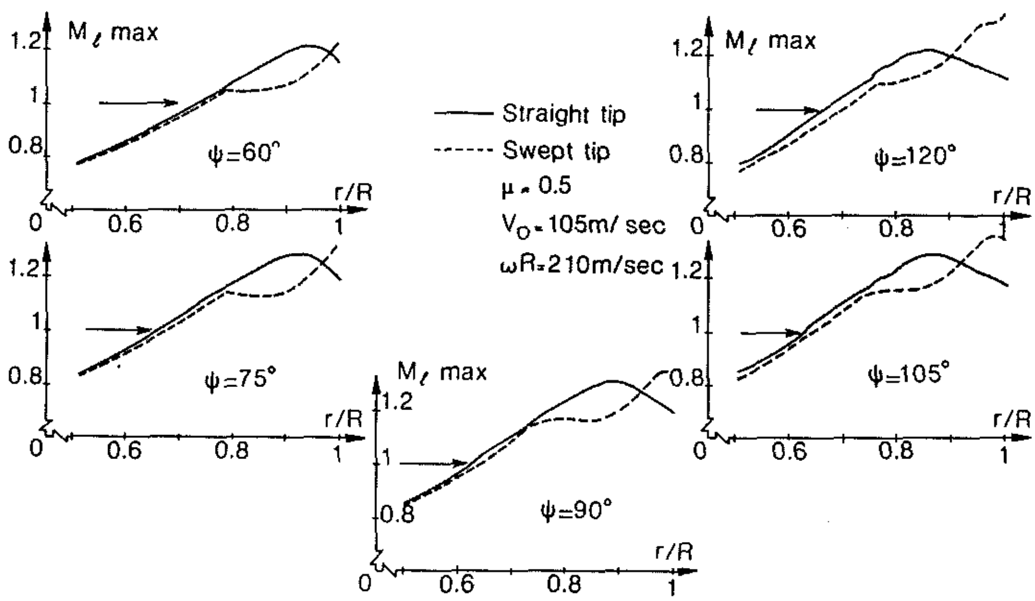

Figure 13 - Spanwise evolution of maximum Mach number

Influence of a swept tip.

The comparison (fig. 14) with experimental results obtained at ONERA shows a good agreement, with however a slight under-estimation of the shock wave intensity at ψ = 120°.

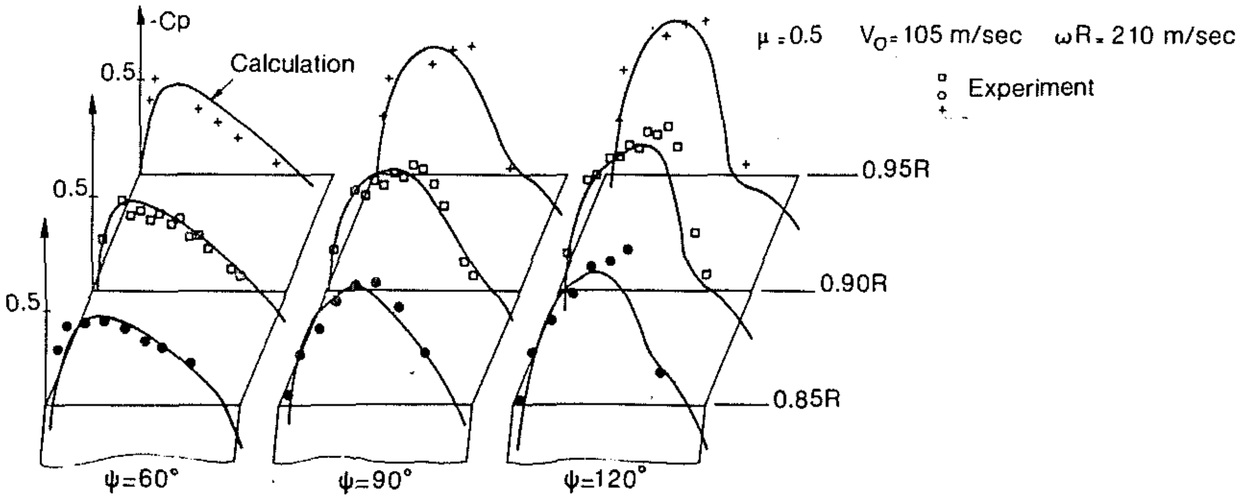

Figure 14 - Comparison between calculation and experiment . Swept tip - Non lifting rotor.

The study of the evolution with azimuth of the pressure coefficient at some chordwise points in spanwise section close to y = 0.9, for the straight tip (fig. 15) and for the swept tip (fig. 16), reveals in the latter case too rapid a disappearance of the shock wave around ψ = 140°, while experimentally it takes place around ψ = 160°.

For the swept blade, the maximum authorized time step is 0.125 degree; 500 quasi steady iterations and 1440 time steps required 1h 25 mm of computing time on CDC 7600.

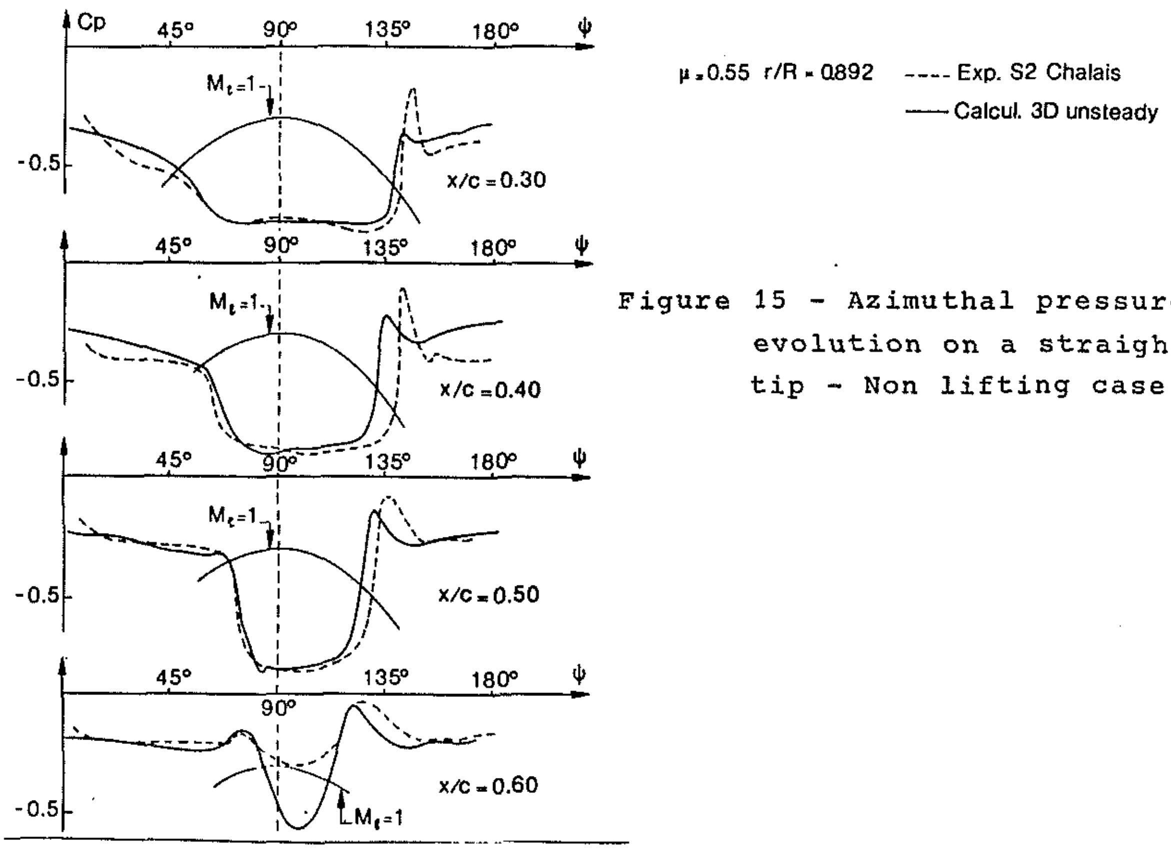

Figure 15 - Azimuthal pressure evolution on a straight tip - Non lifting case.

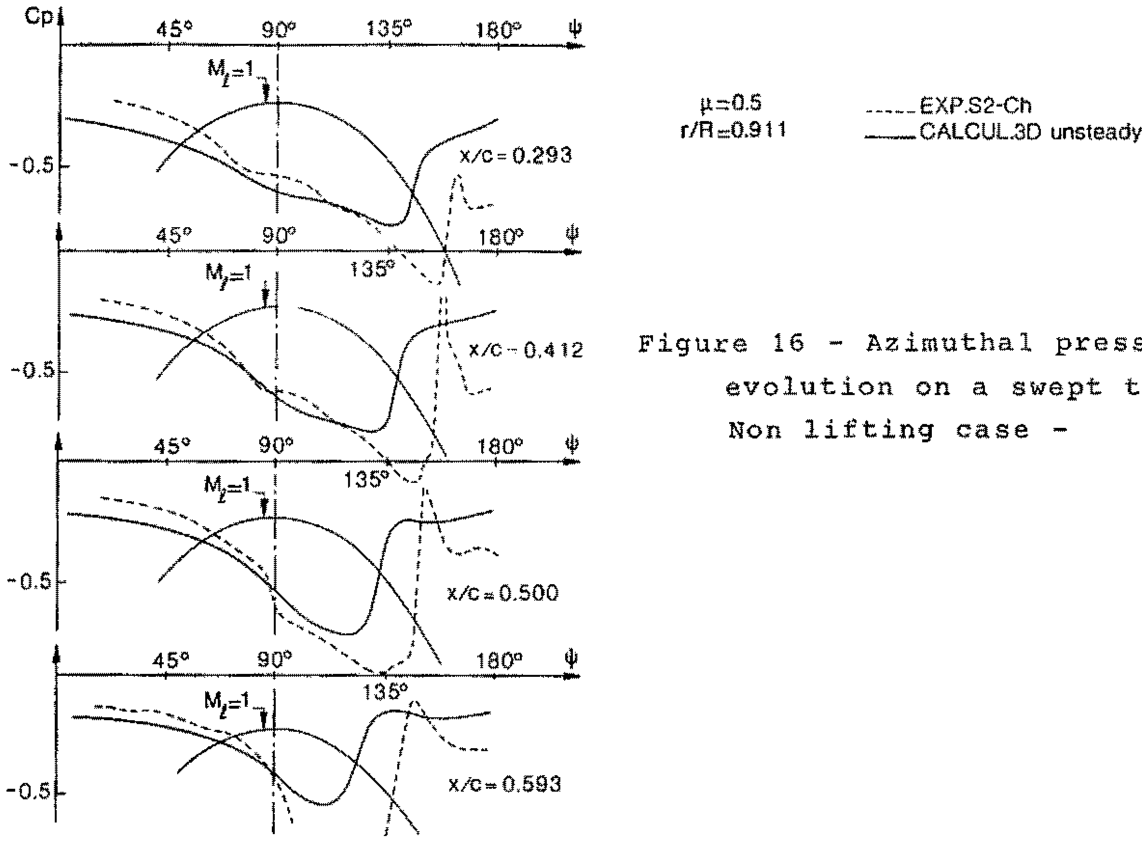

Figure 16 - Azimuthal pressure evolution on a swept tip - Non lifting case -

2.5 - Comparison with other calculation methods

The method developed by the second author [9] is an extension of the method of F.X. Caradonna, of USARTL [10] , to the case of a blade of arbitrary planform. As already mentioned, the unsteady transonic small perturbation equation used is due to M.P. Isom.

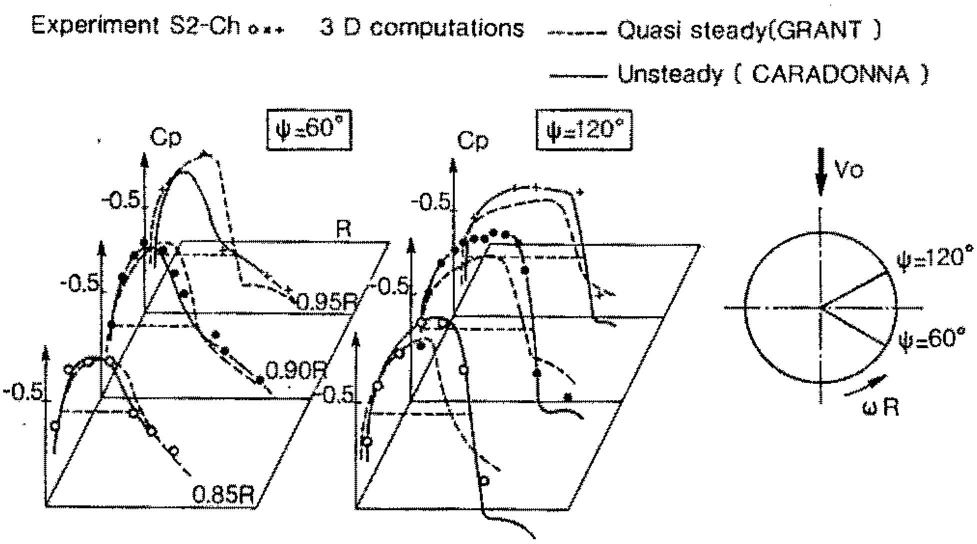

Figure 17 - Pressure distributions on a straight tip. Comparison of various theoretical methods.

Other more complex forms of this equation, in quasi steady form, have been proposed and used in particular at RAE [11] . On figure 17, the Caradonna results are compared with those obtained by Grant for the straight blade. Again it can be seen that taking into account the unsteady character of the flow gives a better agreement with experiments. For the swept tip, where the supersonic zones are smaller and the shocks weaker, the flow exhibits more moderate unsteady character and the RAE method provides a good prediction of the flow at ψ = 60 and 120° (fig. 18) [11] .

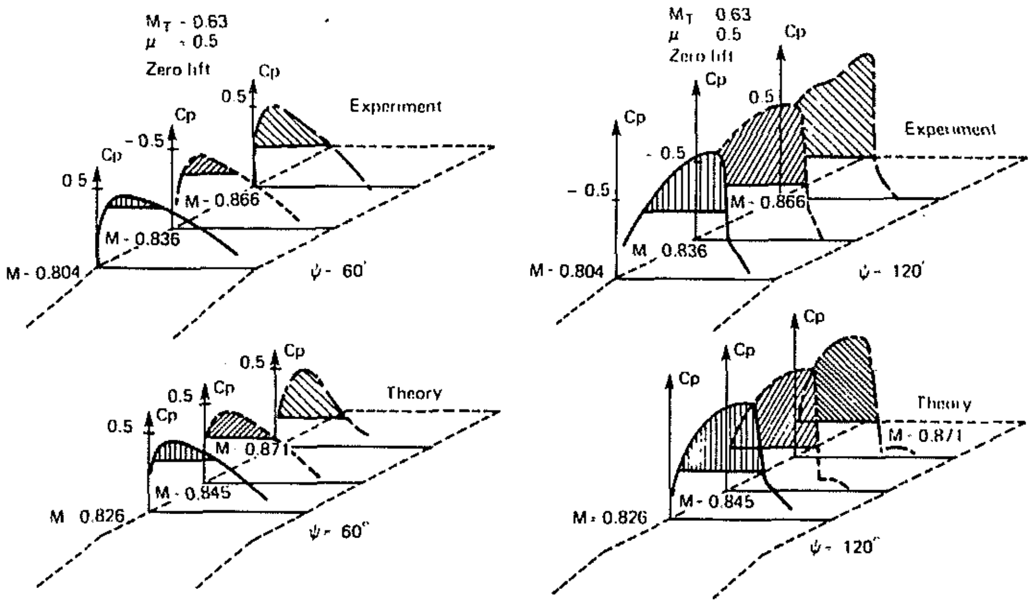

Figure 18 - Tree-dimensional pressure distributions on 30° swept tip (RAE computations).

NASA chose a different approach. M. Tauber and R. Arieli [12] adapted the FLO22 programme of Jameson to the case of a rotating blade. The steady full potential equation is solved in a sheared parabolic coordinates system making it possible to take into account the exact geometry. In this programme, due to the limited number of spanwise stations, the blade tip where interesting phenomena take place is not discretized finely enough to permit detailed representation. Furthermore, the schemes used are non conservative and the shocks do not satisfy jump conditions associated with a shock polar.

We shall note on the Tauber results (fig. 19) the differences with experimental results on the straight blade at azimuths 60° and 120°. These differences can be explained by the absence of unsteady terms in the equation. On the other hand, the complete potential equation should ensure the correct modelization of radial flows. We see the favourable effect of the negative sweep at 120°, which attenuates the pressure peak on the C_p curve for ψ =120°.But, as already noted, the sweep effect, favourable at ψ = 120°, is offset by the unsteady effect favourable at ψ= 60°. This same case has been treated with the ONERA programme, and the results are presented on figure 20.

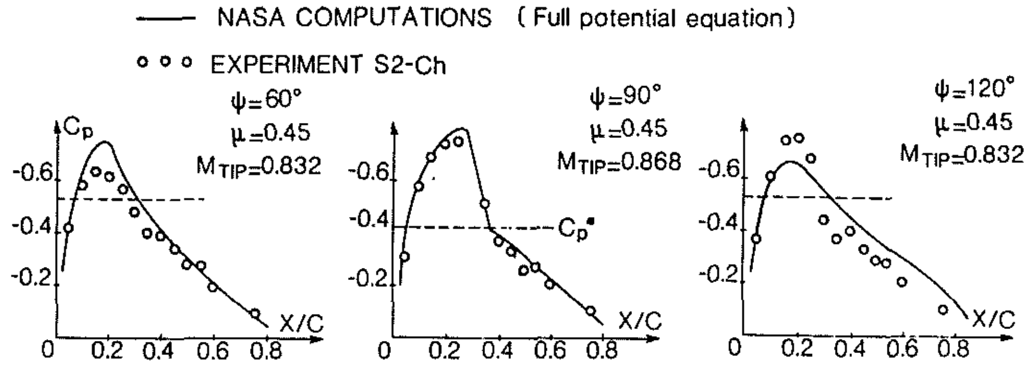

Figure 19 - Comparison between NASA computations and experiment. Straight tip - Non lifting case

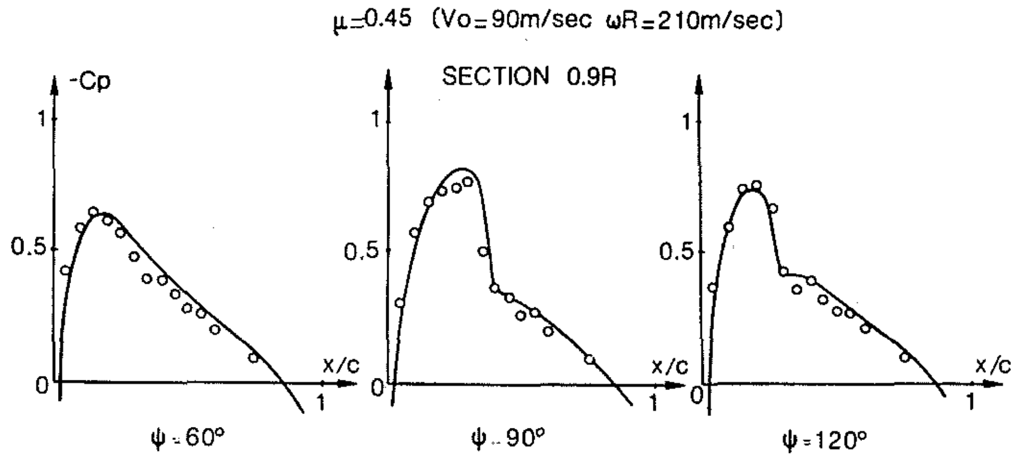

Figure 20 - Comparison between ONERA computations and experiment. Straight tip - Non lifting case

2.6 - Conclusion on theoretical studies

The transonic phenomena taking place on the tip of a helicopter blade in non lifting regime are of a great complexity and fundamentally unsteady, even for small values of advance ratio. A prediction method, to be relevant, must include a modeling of the unsteady and radial terms, a conservative scheme for the discontinuities, a mesh system fine enough to be able to capture the gradients of the solution. To be efficient, the method must incorporate an implicit scheme so as not to be penalized by a stability criterion associated with the size of the smallest cells. The ONERA method of transonic unsteady small perturbations leads to a compromise which makes of it a handy research tool.

The extension of the method to the lifting case is contemplated, but will undoubtedly appear extremely difficult to treat rigorously (modeling of the vortex interaction and of the presence of the other blades).

4 - CASE OF LIFTING ROTOR

The case of lifting rotor has been studied on a 3-bladed rotor model, whose blades were linearly twisted by -12° and articulated in the flapping and lead-lag directions (fig. 21).

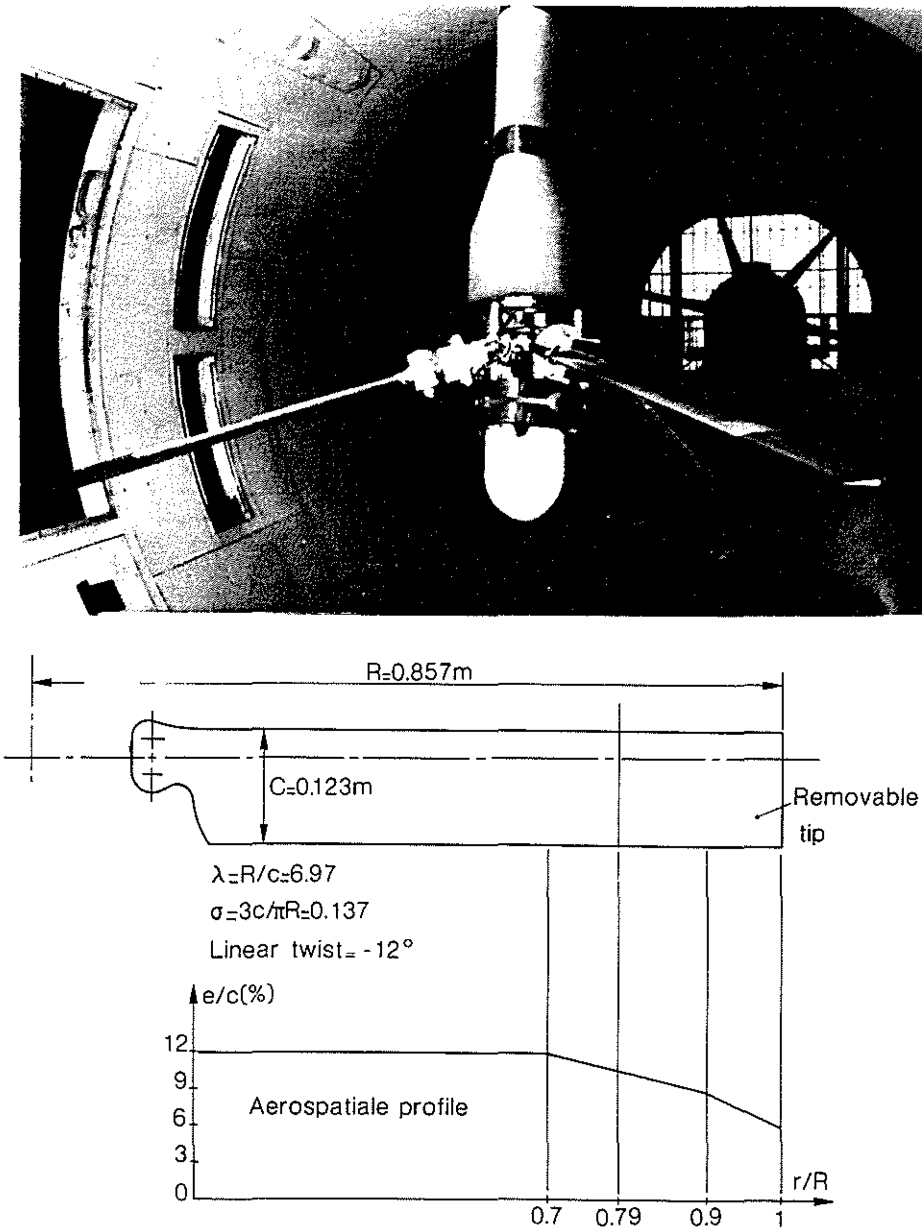

Figure 21 - 3-bladed rotor with removable tips, mounted in the S2 Chalais-Meudon wind tunnel.

There is a collective pitch control but no cyclic pitch control. Figure 21 also gives the main characteristics of the reference straight blade. The blades have profiles defined by the Aérospatiale Company; they are of the 131 family, with a 12% relative thickness up to 0.7 R. There is a first linear decrease of thickness, down to 9% at 0.9 R, and a second one, from 0.9 R to R where the profile is a 13106, of 6% relative thickness. The dimensions and main characteristics of the 13109 profile are to be found in Ref. [13] .

We shall note the low aspect ratio of these blades ($\lambda \simeq 7$) and the high solidity ($\sigma = 0.137$) of this rotor. This is justified by the need of pressure measurements on the blade tips, and thus of having a chord long enough to accommodate a sufficient number of transducers. Moreover, the blades have been designed and built with a view to be as rigid as possible (metallic beam and carbon fibre skin) in order to avoid any excessive aero-elastic deformation. The straight reference tips were equipped with 36 Kulite LDQL absolute pressure transducers, distributed over the three sections 0.85, 0.90, 0.95 R. These transducers were connected, on the upper and lower surfaces, by a T tube, one end of which being closed to perform pressure measurements either on the upper or on the lower surface. References [4] and [5] provide a large amount of informations on the test rig of the S2 Chalais-Meudon wind tunnel and on the technique of acquisition and processing of the data provided by the pressure transducers.

The tests performed to date concern :

- the straight reference blade in hover and forward flight,
- the blade equipped with a sweptback parabolic tip (not instrumented).

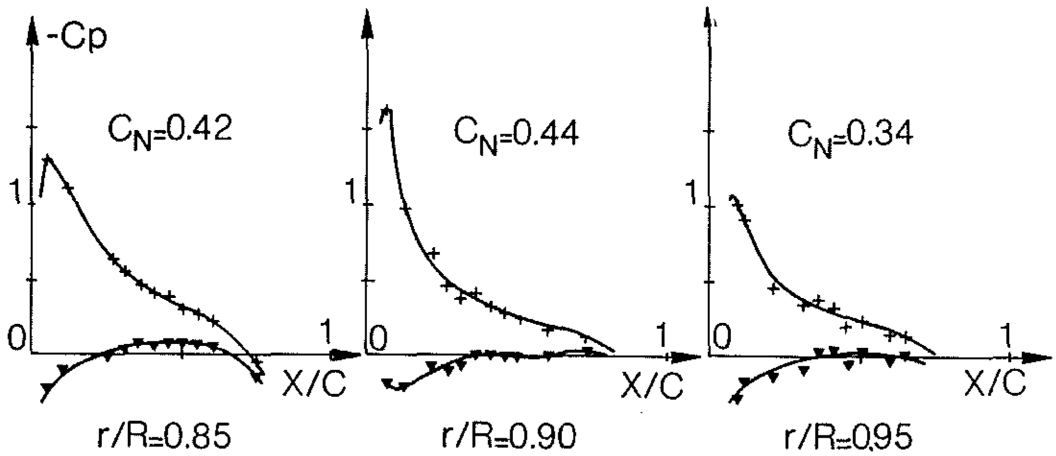

Figure 22 - Experimental blade tip pressure distributions - Straight blade. Hover configuration.

An example of pressure distribution obtained in hover flight configuration is presented on figure 22. This configuration is studied in detail in Ref. [14] , which more particularly describes the velocity field induced by this rotor (measurements by laser velocimetry, and calculation with a free wake method).

4.1 - Study of the straight tip blade

This section is especially devoted to the aerodynamic working conditions of these straight tips in forward flight configurations at velocities from 70 to about 90 m/sec. The set of configurations for which pressure measurements are available is defined on figure 23 by curves providing :

- the evolution of the power $\overline{P}$ to be applied to the rotor as a function of the velocity V_0 in the wind tunnel for several levels of lift, the rotor providing always the propulsive force necessary to balance the drag of a fuselage characterized by $(C_D S)_f / S\sigma = 0.1$;

- the evolution of the power to be applied to the rotor according to the propulsive force provided. (the lift $\bar{L}$ of the rotor and the velocity V_o remaining constant in this case).

This set of configurations allows a first study of the influence of the helicopter forward speed, of the lift force and propulsive force generated by the rotor on the aerodynamic behaviour of the straight tips of a helicopter rotor blade.

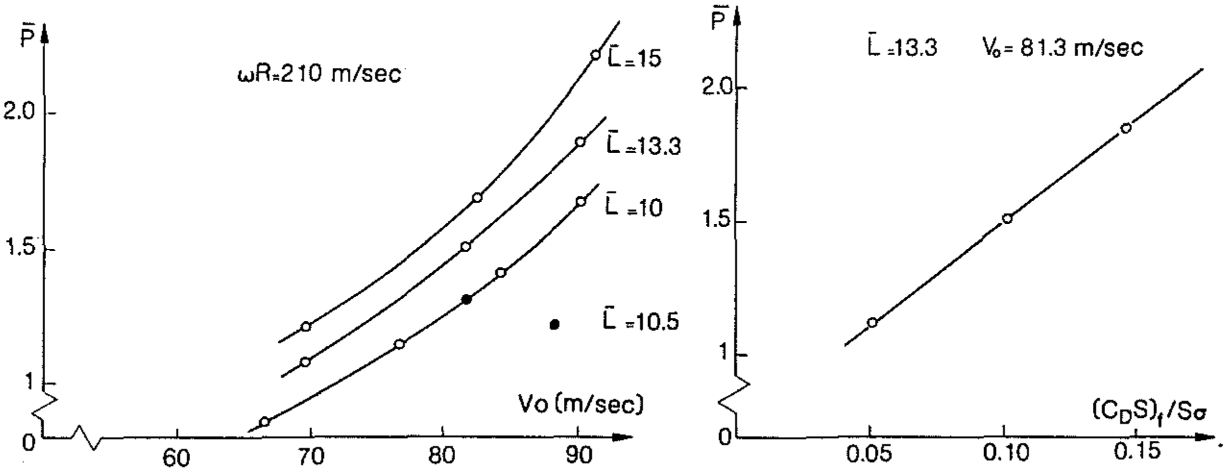

Figure 23 - Power required by the 3-bladed rotor - Pressure measurement configurations.

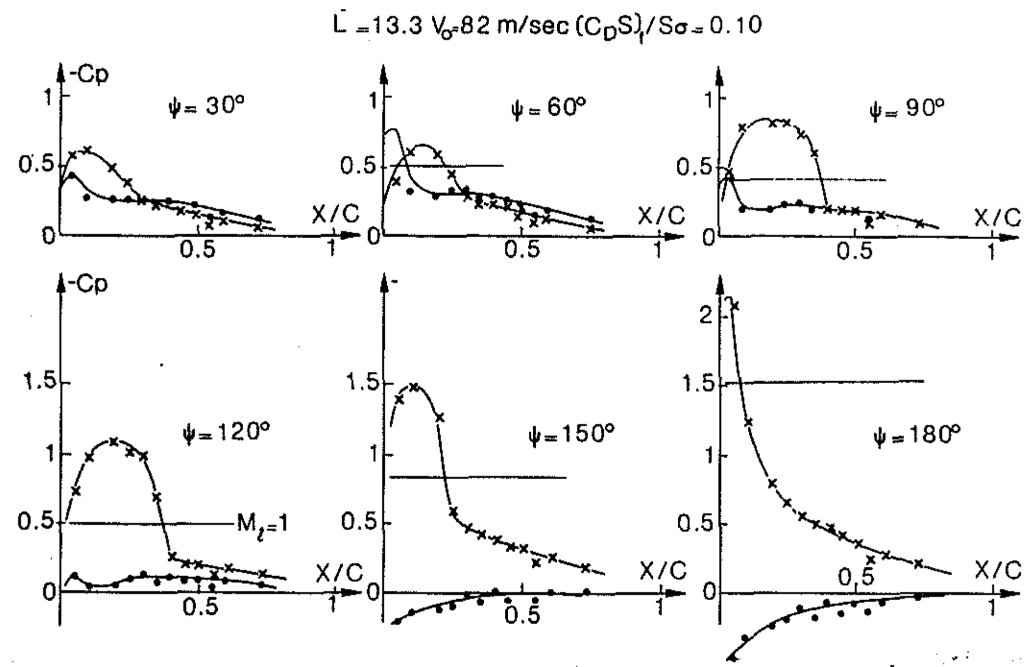

Figure 24 - Pressure distributions on a straight blade tip.

Figure 24 gives an example of pressure distributions obtained on the advancing blade on the 0.9 R section at about 82 m/sec, ($\approx$ 300 km/h) in a configuration where strong transonic flows already occur. Measurements of absolute pressures on a helicopter rotor blade are difficult, and may be slightly inaccurate (of the order of 10 mbar for the transducers used). But they remain mandatory to have a rather clear view of the zones of supersonic flow, of shock intensities and of the conditions of unsteady lift on the various sections of the blade. To this end, figure 25 shows, for the three blade sections where measurements are performed, the evolution of the normal forces C_N (obtained by chordwise integration of unsteady pressure distribution) as a function of incident Mach number $M = (\omega r + V_0 \sin\psi)/a_0$.

We shall note here the very large asymmetry between the upwind blade ($\psi \simeq 180°$) and the downwind blade ($\psi \simeq 0$), which is within the wake of the rotor shaft and the rotor head whose dimensions, in this type of wind tunnel model, are unfortunately much too large relative to those of the rotor disc.

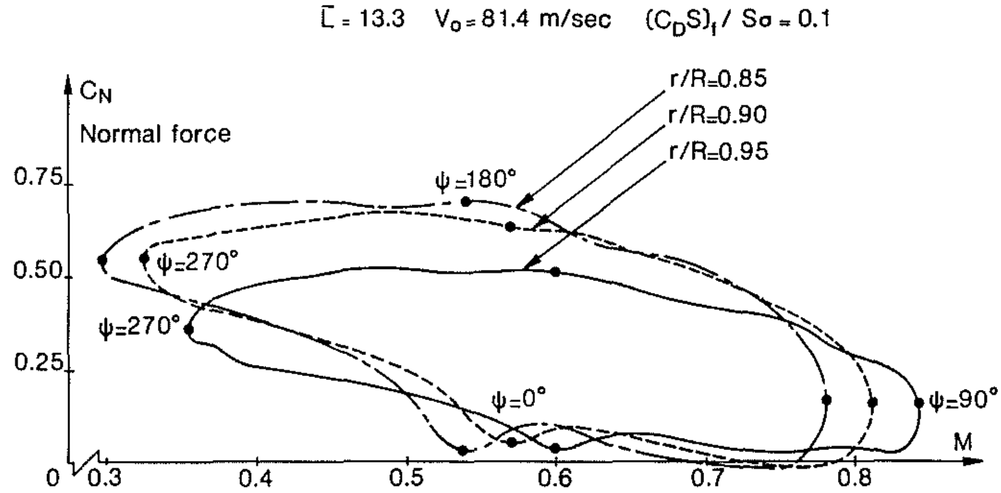

Figure 25 - Aerodynamic working conditions of a helicopter rotor blade tip. 3-bladed OA_C rotor - Straight tip.

4.1.1 - Influence of forward speed

Figure 23 showed that the power to be applied to the rotor increases very fast with the helicopter forward speed. As an example, for a lift $\bar{L}$ of 15, this power increases by 83% between 69.6 m/sec (250 km/h) and 91.1 m/s (328 km/h). Figure 26 shows that, on the 0.9 R section, located at 0.7 chord from the blade tip, the zones of supersonic flow extend more and more along the profile chord, that they are present on a larger and larger azimuthal sector and that they are characterized by a higher and higher maximum local Mach number, reaching 1.4 at V_0 = 91.1 m/s. When the helicopter speed increases and if we want to ensure the same lift and the propulsive force necessary to balance the fuselage drag, the blade sections close to the tip have to work in even more difficult conditions of Mach and lift, as shown on figure 27. The drag divergence Mach numbers and maximum lifts obtained during two-dimensional tests of the 13109 Aérospatiale profile at the S3 wind tunnel in Modane are also plotted on the figure. We can see that above V_0 = 69.9 m/s the profile in the 0.9 R section works above its 2D. drag divergence Mach number, which can only increase the local aerodynamic drags and the power necessary to drive the rotor.

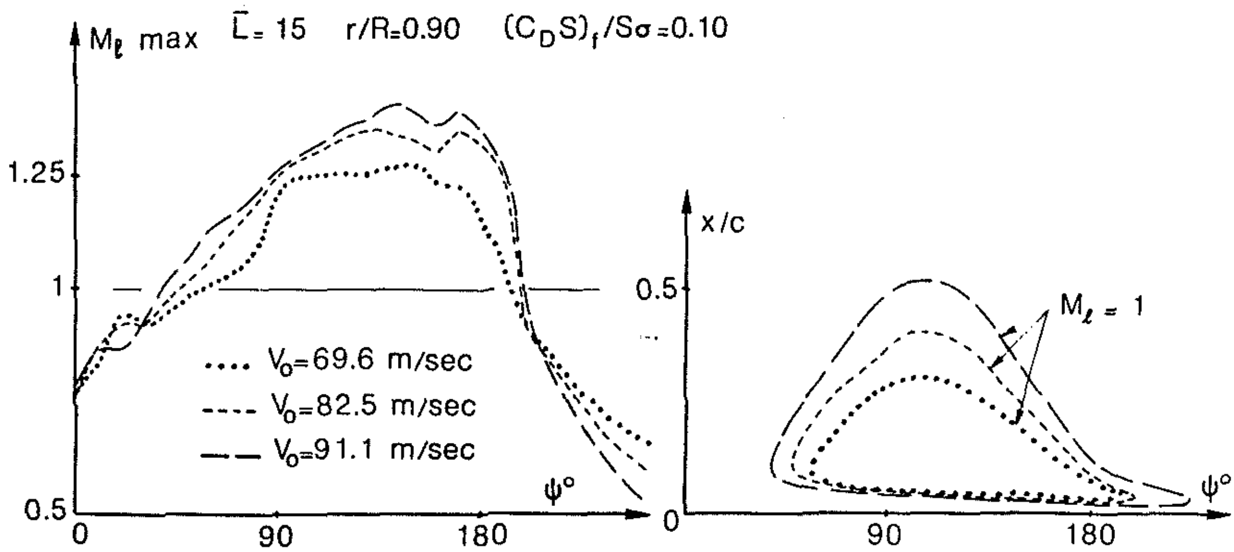

Figure 26 - Evolution of the zones of supersonic flow with the forward speed V_o.

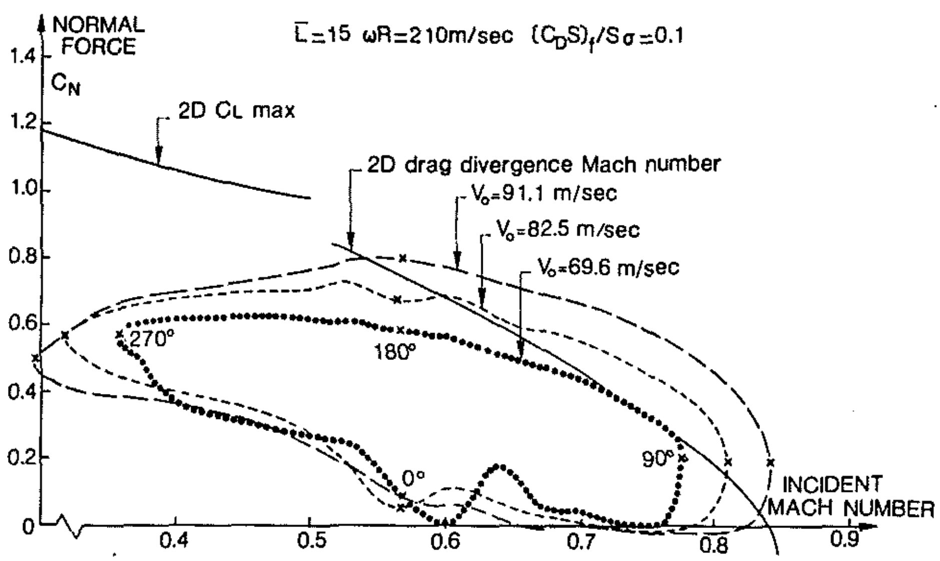

Figure 27 - Evolution of local loads - (0.9 R section).

4.1.2 - Influence of the lift generated by the rotor

Figure 28 illustrates the influence of the rotor lift on the aerodynamic working conditions of this same section at 0.9 R. Forward speed V_o is about 82 m/sec (295 km/h), and on the three lift cases presented the propulsive force necessary to balance the drag of a fuselage characterized by $(C_D S)_f / S\sigma = 0.1$ is always insured. The increase of overall lift of the rotor is expressed by an increase of local lift of the profile, particularly in the sector of upwind blade, between ψ = 90° and 270°. This increase of local lift is more critical in the 90° - 180° sector, where the drag divergence Mach number of the profile is exceeded.

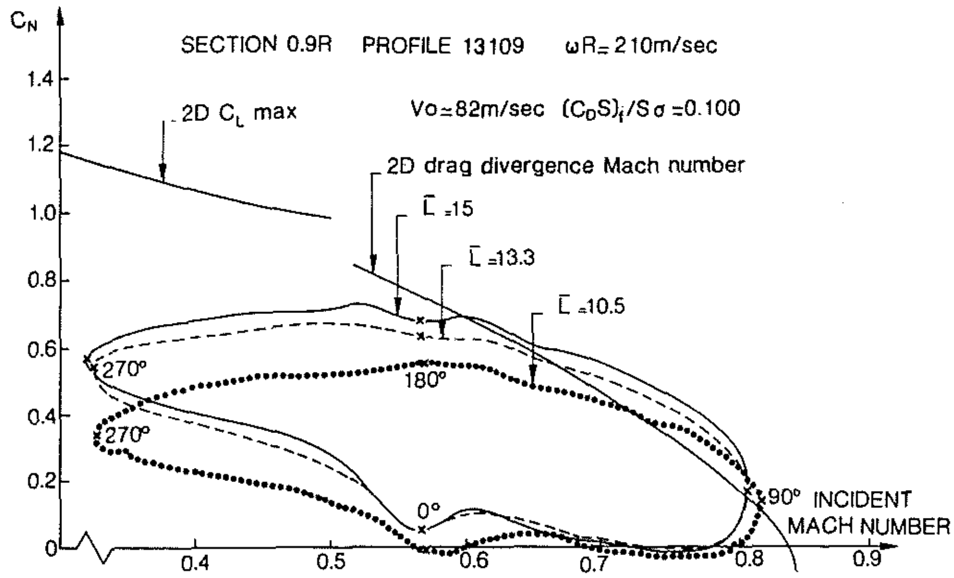

Figure 28 - Influence of the lift on the blade tip aerodynamic working conditions.

4.1.3 - Influence of the propulsive force provided by the rotor

Figure 29 shows the influence of the propulsive force provided by the rotor on the aerodynamic working conditions in the 0.9 R section (the rotor lift and forward speed V_o remaining constant). The increase of propulsive force is expressed, as for the increase of rotor lift, by increases of local loads on blade tips, especially on the whole upwind part of the rotor disc (90° - 180° - 270°), more particularly penalizing in the 90°-180° azimuthal sector.

Thus, the measured pressure distributions make it possible to well understand under which conditions the blade tips work; they can already provide indications for improving the operation at high speed of this reference rotor. As an example, the figures presented show that the profile located at 0.9 R is ill adapted to high speeds, and that a law of relative thickness of the profiles which would decrease more rapidly than the one chosen for this rotor could likely improve the performance of this rotor model. The set of results already acquired could serve as a basis for an experimental comparison with those that will be obtained later with new shapes of blade tip. We shall in particular know in which azimuthal sector the new tip has better or less good performance than the straight reference tip, and if the new tip actually meets the desired local improvements.

The results acquired will also serve as a basis for comparisons with results of calculations of pressure distributions on helicopter rotors in lifting configurations.

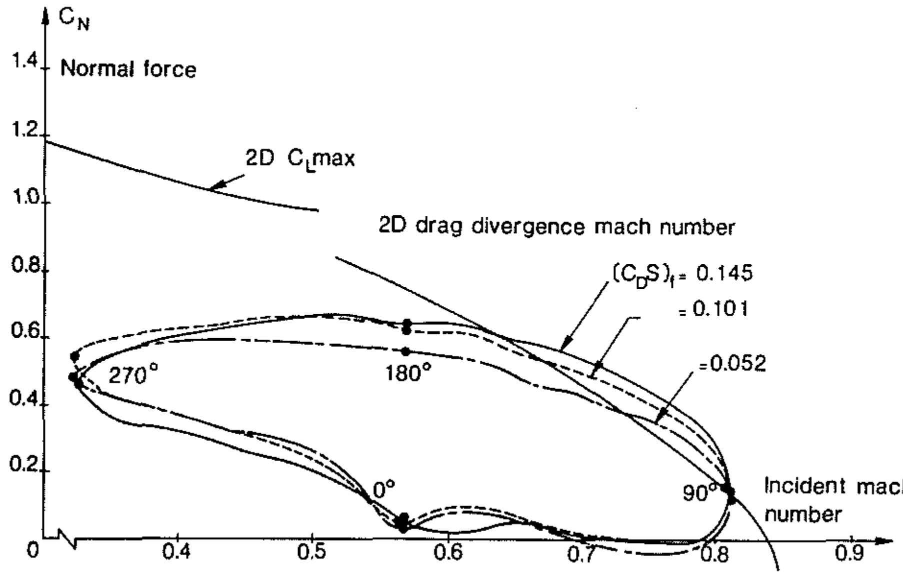

Figure 29 - Influence of the propulsive force level on blade tip aerodynamic working conditions.

4.2 - Study of the sweptback parabolic blade tip

A sweptback parabolic blade tip, whose shape is presented on figure 30, has been defined with a view to improve the performance of a rotor working at a high forward speed.

4.2.1 - Criteria for the choice of this blade tip shape

The study of the non lifting 2-bladed rotor with sweptback tip (see section 3) had showed that a classical 30° swept tip entails for the rotor a lesser expense of power (see for instance figure 21 of Ref. [5] or figure 24 of Ref. [1] , but that there exists on the external edge of this tip accelerations of the flow which may be penalizing as regards aerodynamic drag. So this external part of the swept tip should be improved. The interest of using conventional swept tips with or without chordwise taper has been proved by wind tunnel tests on a full scale model [15] or at reduced scale e.g. [16] , and this type of tip has been adopted by the Sikorsky Company on its various aircraft (Black Hawk or S76).

The idea of using a parabolic leading edge arose after the study of tests, carried out as soon as 1970 in the ONERA S3 Chalais-Meudon wind tunnel on half wings at the wall, equipped with various tips. The analysis of these tests by Vincent de Paul, figure 31, shows results obtained with and without a parabolic tip. We clearly see that this shape reduces considerably the pressure peaks at the wing tip, as can be observed at M_O = 0.85 for instance by an appreciable gain on the wing drag. So we decided to modify the external part of a classical sweptback tip with straight leading edge by giving the leading edge a parabolic shape, which entails a gradually increasing local sweep angle.

The blade tip finally retained (see fig. 30) for tests on a 3-bladed rotor is thus made of a leading edge with constant 30° sweep angle over 0.35 c (between 0.9 and 0.95 R), then with a varying-sweep angle over 0.35 c (between 0.95 R and R), with adoption of a parabolic line bringing the leading edge of the last profile of the tip at 0.8 c behind the straight part of the blade. The tip profile has a chord half the length of that of the straight part of the blade. This shape has been presented in 1978 in Ref. [17] .

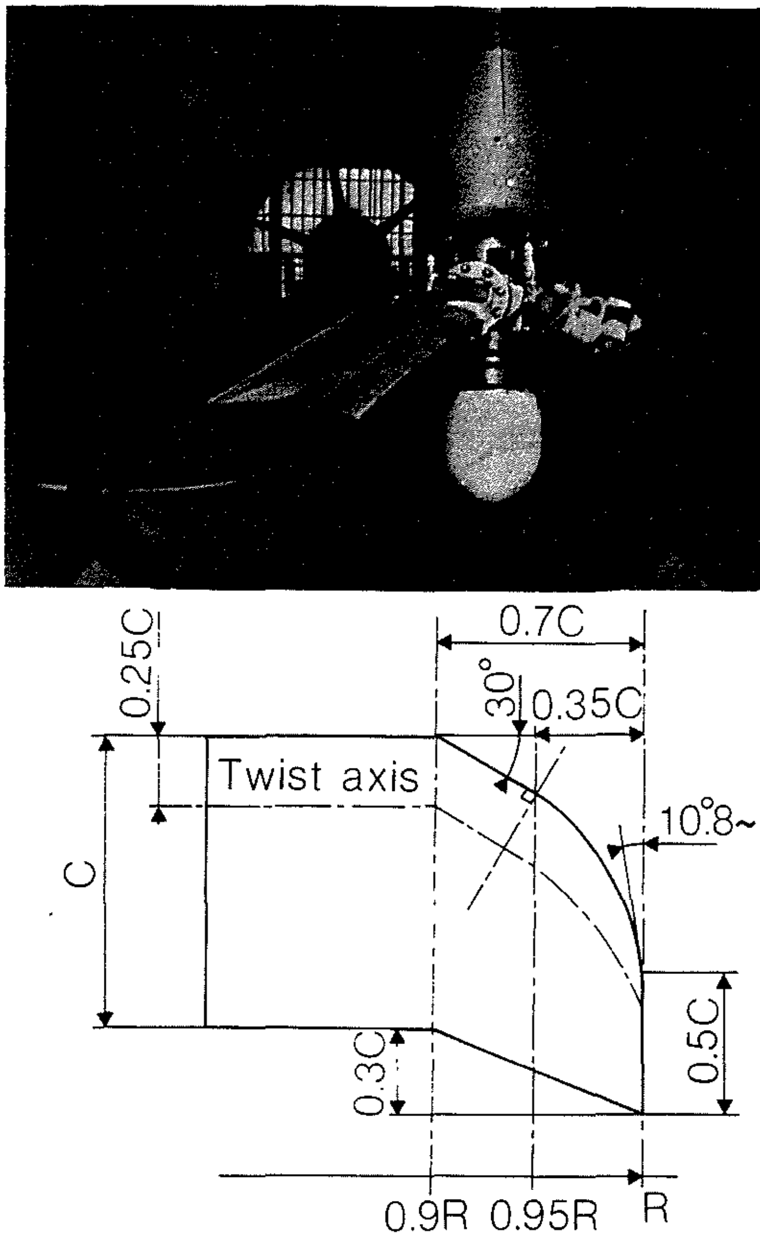

Figure 30 - Sweptback parabolic tip on the 3-bladed rotor.

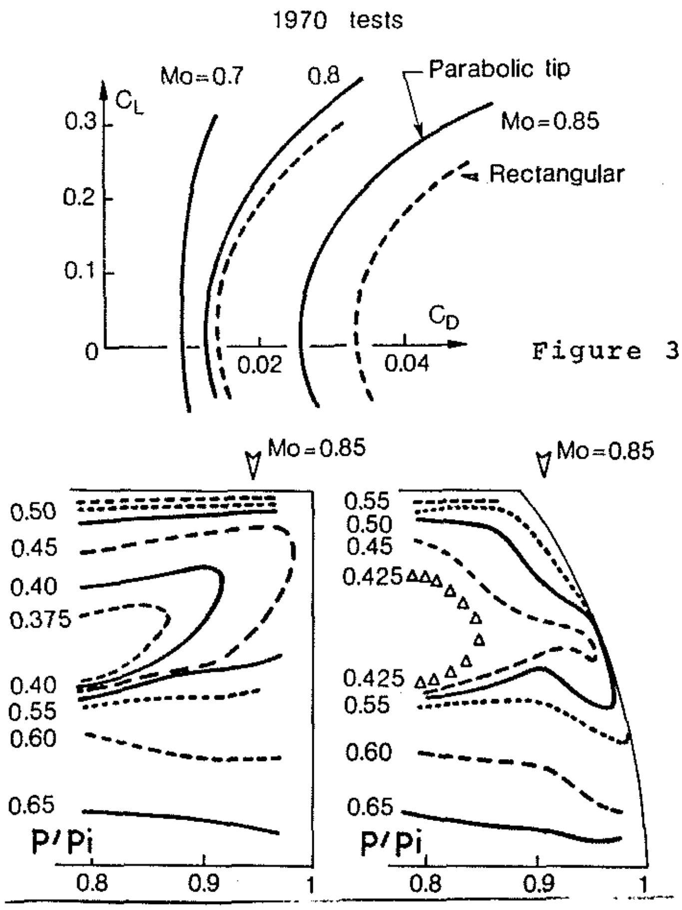

Figure 31 - Half wing with parabolic tip (λ = 6).

To make sure of the validity of this shape, calculations have first been performed on half wings at the wall, to compare the influence of this new tip and of a sweptback tip with constant chord on pressure distributions and local Mach numbers. The calculations were performed with a computer programme developed at ONERA, which solves the complete velocity potential equation [18] . The results obtained (fig. 32, 33) show that, on the sweptback parabolic tip, there is no flow re-acceleration in contrast to the sweptback tip with constant chord, which is expressed, on the spanwise distribution of maximum local Mach number, by a very gradual decrease of this maximum local Mach number towards the blade tip.

Calculations have also been performed by RAE at Farnborough by means of its prediction programme of pressure distributions on helicopter rotor blades (quasi steady hypothesis), described in Ref. [11] . Figure 34 shows the spanwise distributions at azimuth 90° of maximum Mach number along the blade equipped with the conventional rectangular tip or the sweptback parabolic tip defined by ONERA. The results clearly show (in this case of zero lift) that the problems related to the presence of transonic flows on the advancing blade are greatly reduced. We should note the very large reduction of maximum Mach number at the 30° blade kink at 0.9 R along the blade. As early as 1978, RAE has shown [11] the interest of rounding up the leading edge line over part of the sweptback tip or over almost its whole length.

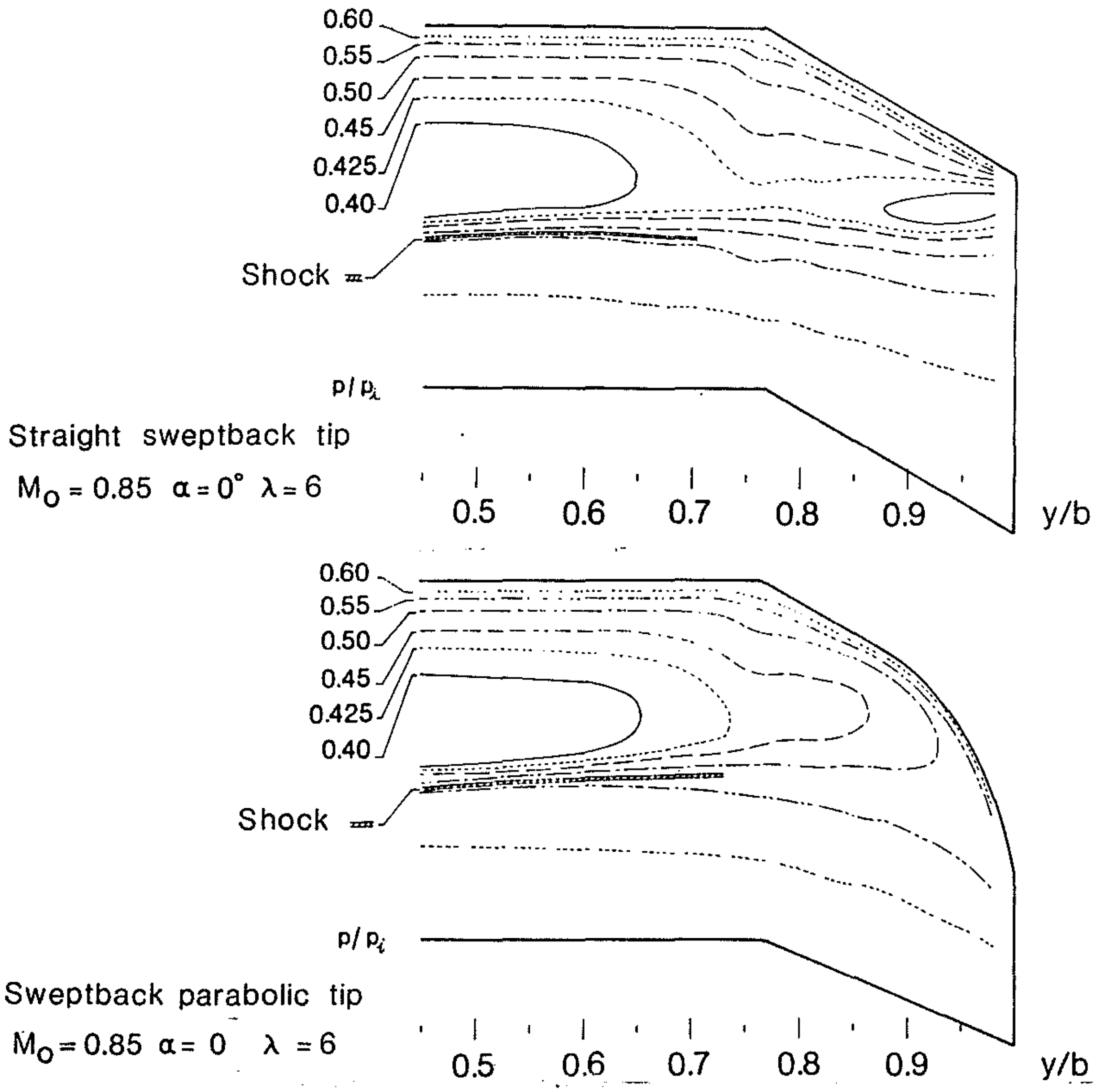

Figure 32 - 3D steady computations - Full potential equation.

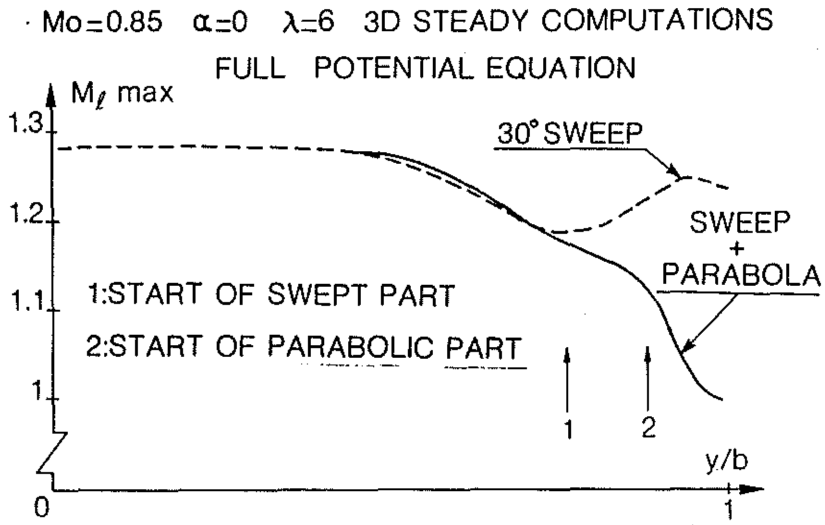

Figure 33 - Influence of a modification of the swept part of a wing tip on the maximum local Mach numbers.

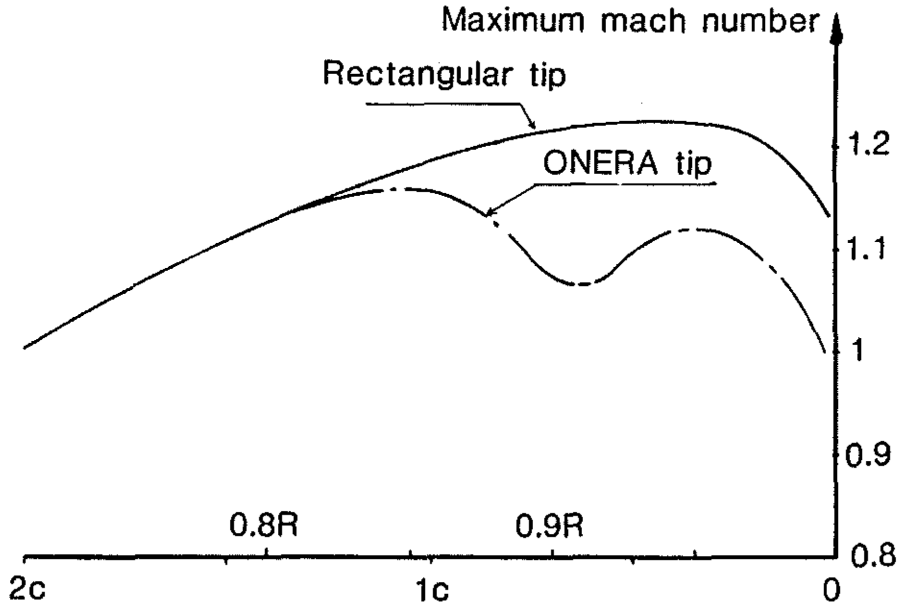

Figure 34 - Maximum Mach number on the upper surface of the blade tip at Ψ = 90°. Zero lift - μ = 0.4 - M_T = 0.64 - 3D quasi steady computations -

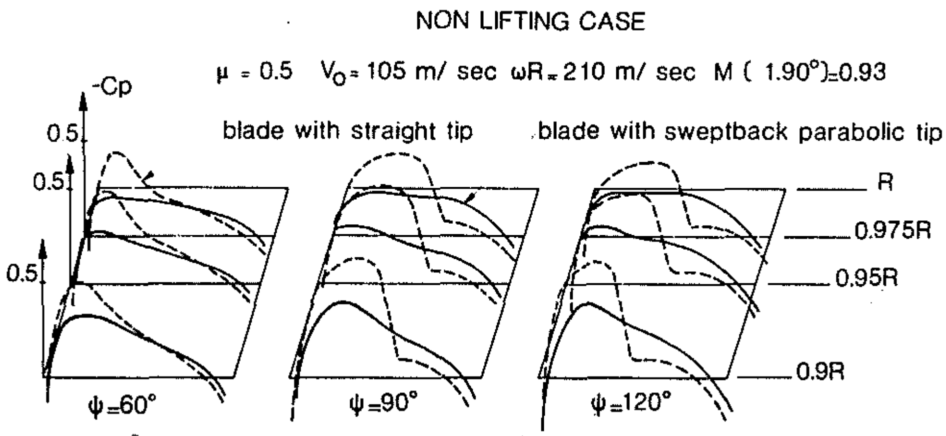

Figure 35 - Unsteady calculations with ONERA Programme on straight and sweptback parabolic tips.

Lastly, calculations have just been performed with the unsteady programme described in section 3.2. Figure 35 confirms the interest of the planform adopted by ONERA, showing for instance that at azimuths 60°, 90°, 120° there is no shock over almost all the sweptback parabolic tip, while there appear very strong ones on the straight tip. Figure 36a, which presents the spanwise variation of maximum local Mach numbers, shows that the beneficial effect of the sweptback parabolic tip extends inside the span, up to about 0.7 R (i.e. about 2 chords from the blade tip). We shall remark that very close to the blade tip there remains a very sharp (but very localized) re-acceleration of the fluid, which is confirmed by the plotting of iso-Mach lines for ψ = 90° (fig. 36b). It is probable that this could be attenuated if the leading edge line ended tangent to the blade chord.

The same figure also presents the result obtained on a constant chord, sweptback wing. The parabolic part of the tip actually suppresses all of the overexpansion appearing in this case.

The above discussion proves that the new blade tip should improve the aerodynamic behaviour of the tip of a helicopter blade in the advancing blade sector, but it is not quite obvious that it improves the total performance of the rotor; that is why it has been tested on the 3-bladed rotor of the S2-Ch wind tunnel

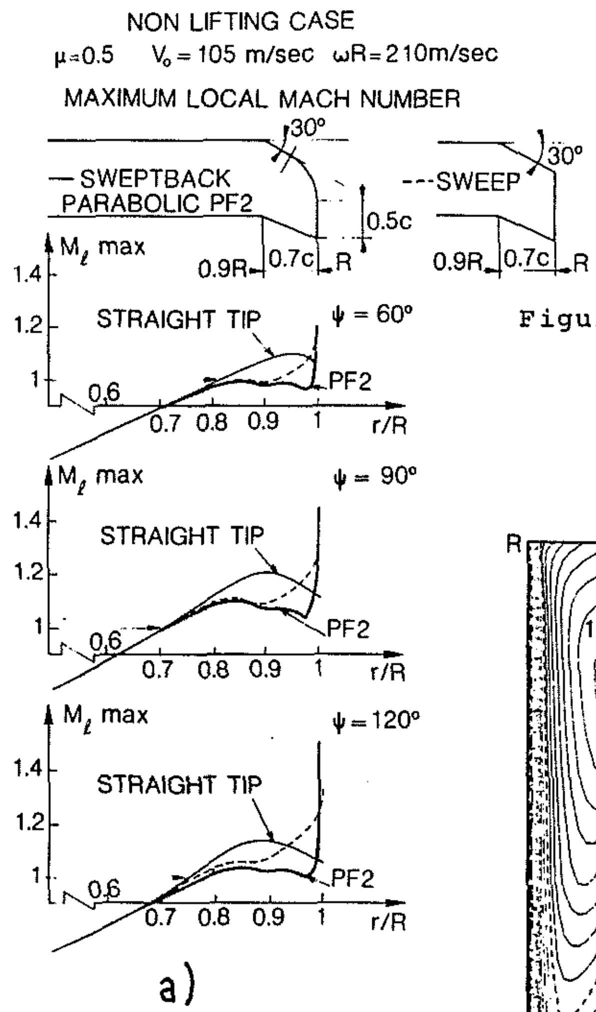

Figure 36a - Comparison of straight, sweptback and sweptback parabolic tips.

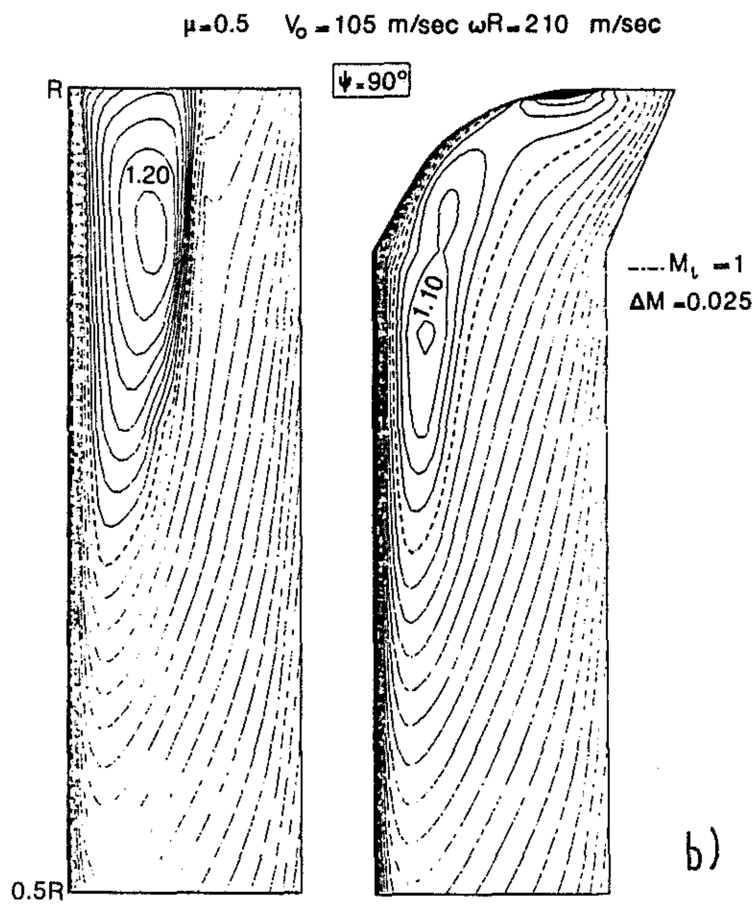

Figure 36b - Iso-Mach lines at $\Psi = 90°$.

4.2.2 - Results on the total performance of the rotor

Figures 37 through 40 show a comparison of the total performance of the 3-bladed rotor, acquired during tests at S2Ch on blades with straight or parabolic tips (such as defined on figure 30).

Figure 37 shows that, whatever the forward speed above 69 m/sec ($\simeq$ 250 km/h) and up to 91 m/s ($\simeq$ 325 km/h) at least, the rotor equipped with sweptback parabolic tips will require less power, the tests being conducted at three lift levels ($\bar{L}$ = 10, 13.3 and 15), the rotor always ensuring the propulsion necessary to balance the drag of a fuselage characterized by $(C_D S)_f / S\sigma$ = 0.1.

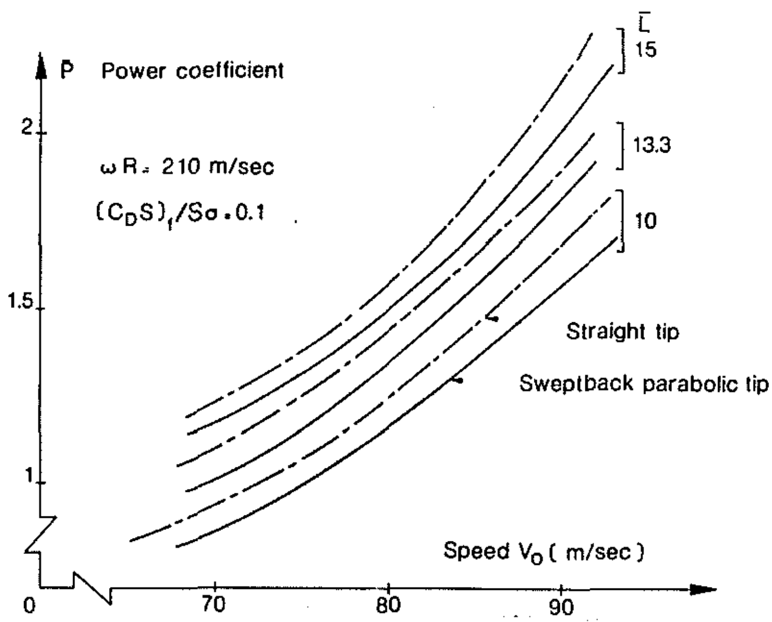

Figure 37 - Power required by the rotor for various forward speeds at various values of lift.

Figure 38 shows that at 83 m/sec ($\simeq$ 300 km/h), which represents approximately a limiting speed of continuous flight for present-day conventional pure helicopters, the power gain brought by the sweptback parabolic tip is important up to a lift coefficient of at least 16.7, which may allow the designer to consider increasing the helicopter payload for the same power.

Figure 39 shows that around this speed of 300 km/h and for a lift $\bar{L}$ = 13.3, the power gain is practically of the same order whatever the fuselage carried by the rotor $(0.05 < (C_D S)_f / S\sigma < 0.15)$, which may authorize increasing the fuselage useful volume for the same power.

Lastly, figure 40 shows that there is still a slight gain in hover flight, as the figure of merit of the rotor equipped with sweptback parabolic tips is slightly higher than that equipped with straight tips.

One should not indeed draw hasty conclusions about the gain to be expected in a real helicopter rotor, as the rotor model tested has very rigid blades, of small aspect ratio; flight tests would be more instructive.

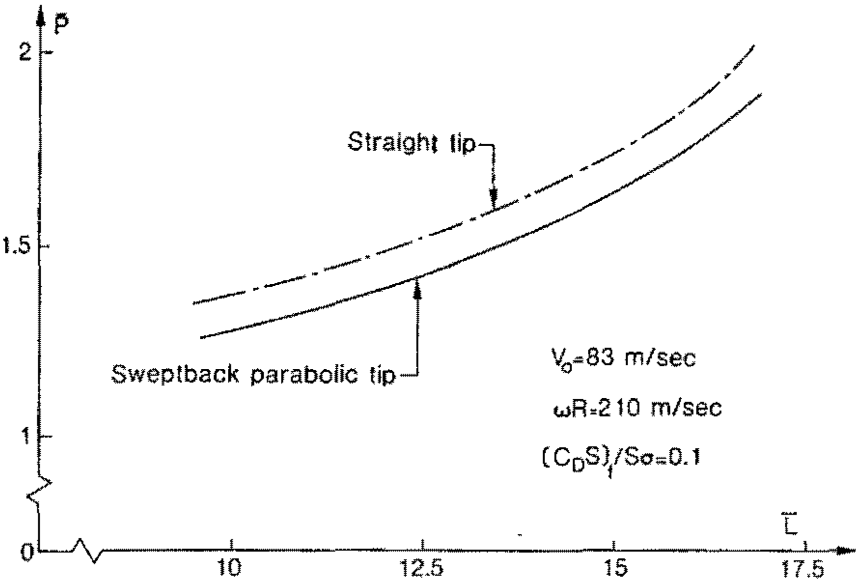

Figure 38 - Power required by the rotor for various lift at a given forward speed.

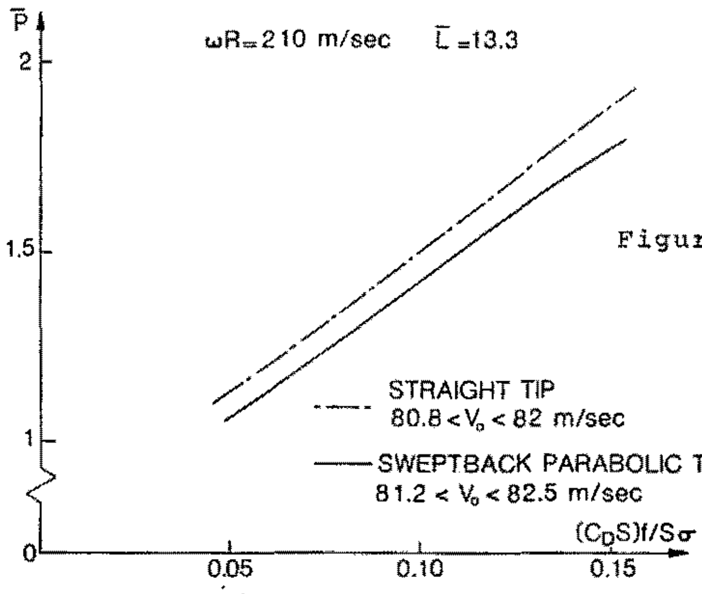

Figure 39 - Power required by the rotor driving various fuselages.

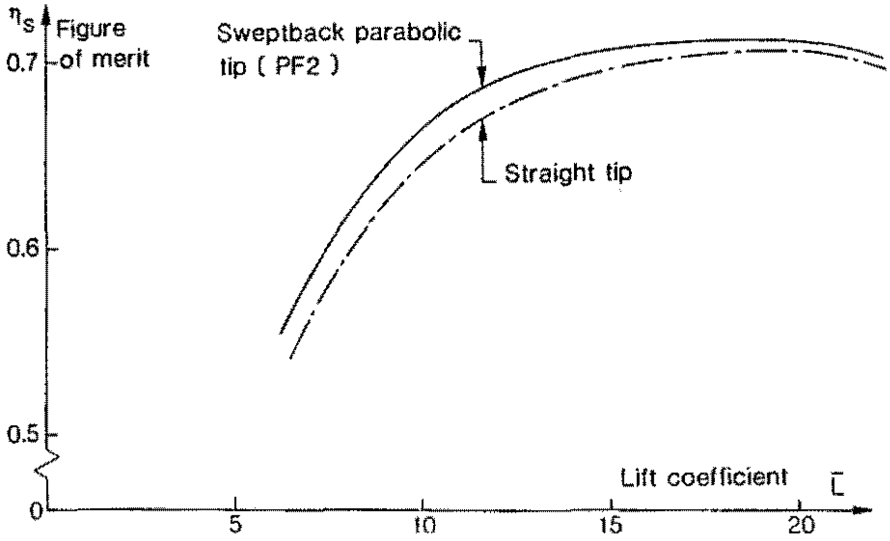

Figure 40 - Influence of the blade tip shape on the rotor figure of merit (hover flight).

Moreover, the sweptback parabolic tip defined and tested at ONERA can probably be still improved; in this respect, it will be remembered that the idea of optimizing the working conditions of the advancing blade from calculations at zero lift proved fruitful for increasing the total performance of a rotor. It would also be very interesting to perform pressure measurements on these newly defined tips, to confirm the causes of the improvements observed.

5 - CONCLUSIONS

The theoretical and experimental research carried out at ONERA on helicopter blade tips in non-lifting and lifting configurations made it possible to improve our knowledge of their flows environment, and to contribute in the improvement of prediction means and in the increase of the performance of helicopter rotors. The influence of many other parameters remains to be investigated, such as, for instance, a non linear twist which would, in particular, yield a better performance in hover flight. The study of flexible blades will be of a still greater complexity, especially if as intended in Ref.[19], a sweptback tip is used to modulate the blade twist according to its azimuthal position. To pursue the optimization of blades in their actual working conditions, it is fundamental to have available codes for computing pressure distributions in lifting conditions, in more or less complicated form; the rigorous calculation, even in ideal fluid, remains however a far fetched objective as it will surely require very large computing facilities and very lengthy calculations.

REFERENCES

[1] - J.J. Philippe, C. Armand - ONERA Aerodynamic Research Work on Helicopters, in AGARD CP 233 - Paper n°22 (1977), "Symposium on Rotorcraft Design" - in French in "La Recherche Aérospatiale N° 1978-6.

[2] - J.J. Thibert, J. Gallot - Advanced research on helicopter blade airfoils, 6th European Rotorcraft and Powered Lift Aircraft Forum, Bristol, Sept. 1980.

[3] - J.J. Costes - Calcul des forces aérodynamiques instationnaires sur les pales d'un rotor d'hélicoptère - AGARD Report n° 595 and Recherche Aérospatiale N° 1972-2 (trad. NASA TT-F-15039, 1973).

[4] - F.X. Caradonna, J.J. Philippe - The flow over a helicopter blade tip in the transonic regime, Vertica, vol. 2 N°1, 1978 - (Paper presented at the Second European Rotorcraft and Powered Lift Aircraft Forum, 1976).

[5] - B. Monnerie, J.J. Philippe - Aerodynamic problems of helicopter blade tips, Vertica, vol. 2, pp. 217-231 (Paper presented at the Third European Rotorcraft and Powered Lift Aircraft Forum, 1977).

[6] - M.P. Isom - Unsteady subsonic and transonic potential flows over helicopter rotor blades, NASA CR-2463, 1974.

[7] - W.F. Ballhaus, A. Jameson, J. Albert - Implicit approximate - factorization schemes for the efficient solution of steady transonic flow problems, AIAA paper n°77-634, June 1977.

[8] - E.M. Murman - Analysis of embedded shock waves calculated by relaxation methods, Proceedings of AIAA conference on Computational Fluid Dynamics, Palm Springs, July 1973.

[9] - J.J. Chattot - Calculation of three-dimensional unsteady transonic flows past helicopter blades, NASA TP, AVRADCOM TR 80-A-2 (AM), 1980.

[10] - F.X. Caradonna, M.P. Isom - Numerical calculations of unsteady transonic flow over helicopter rotor blades, AIAA Journal, vol. 14 N°4, April 1976.

[11] - J. Grant - The prediction of supercritical pressure distributions on blade tips of arbitrary shape over a range of advancing blade azimuth angles, 4th European Rotorcraft and Powered Lift Aircraft Forum, Stresa, Italia, Sept. 1978.

[12] - R. Arielli, M.E. Tauber, Computation of subsonic and transonic flow about lifting rotor blades, AIAA Paper n°79-1667, Atmospheric Flight Mechanics Conference, August 1979.

[13] - US Army Helicopter Design Datcom, vol.1 Airfoils (May 1976), Boeing Doc. N°0210-1197-1.

[14] - E. Horowitz, J.M. Pouradier- Aerodynamic study of a hovering rotor, 6th European Rotorcraft and Powered Lift Aircraft Forum, Bristol, Sept. 1980.

[15] - R.H. Stroub, J.P. Rabbott, C.F. Niebanck - Rotor Blade Tip Shape Effects on Performance and Control Loads from Full-Scale Wind Tunnel Testing. Journal of the A.H.S. - Vol. 24 Nr. 5, October 1979.

[16] - W.H. Weller - Experimental Investigation of Effects of Blade Tip Geometry on Loads and Performance for an Articulated Rotor System, NASA TP 1303, AVRADCOM TR 78-53 (Janvier 1979).

[17] - J.J. Philippe, P. Lafon, J.C. Bohl - Etudes expérimentales d'aérodynamique instationnaire sur des maquettes de rotors d'hélicoptère en soufflerie, Colloque d'Aérodynamique Appliquée de l'AAAF, Marseille, Novembre 1978 - (NT AAAF 79-21).

[18] - J.J. Chattot, C. Coulombeix, C. Tome - Calculs d'écoulements transsoniques autour d'ailes, La Recherche Aérospatiale n° 1978-4, English translation ESA-T.T.561 (1979).

[19] - R.H. Blackwell and al. - Wind tunnel evaluation of aeroelastically conformable rotors, 36th Annual Forum of the AHS, Washington, May 1980.

- MAIN NOMENCLATURE -

α	incidence (°)
M	incident unsteady Mach number : $(\omega r + V_o \sin\psi)/a_o$
a_o	speed of sound (m/sec)
M_l	local Mach number on the profile
V_o	wind velocity in the wind tunnel (m/sec)
ω	angular velocity of the rotor (rad/sec)
r/R	relative radius of a blade section
R	rotor radius (m)
y/b	relative spanwise position of a section of half wing at the wall
ψ	blade azimuthal position (°)
p	pressure (Pa)
p_o	static pressure (Pa)
p_i	stagnation pressure (Pa)
φ	sweep angle (°)
$\bar{L}$	rotor lift coefficient : $100\,Fz / (1/2\,\rho\,(\omega R)^2 S\sigma)$
$\bar{P}$	coefficient of power required by the rotor : $100\,P / (1/2\,\rho(\omega R)^3 S\sigma)$
σ	rotor solidity : $3c/\pi R$ (for a 3-bladed rotor)
S	area of rotor disc (m^2)
$(C_D S)f$	equivalent drag area of a fuselage (m^2)

μ	advance ratio : $V_0/\omega R$
C_p	pressure coefficient : $(p-p_0)/1/2\ \gamma p_0 M^2$
x/c	chordwise relative position on a profile
M(1,90°)	Mach number at the tip of advancing blade
C_L	lift coefficient of a profile
C_N	normal force coefficient of a profile
η_s	figure of merit : Froude theoretical power/actual power required by the rotor